Inorganic Chemistry

Forum Article

pubs.acs.org/IC

Lanthanides and Quantum Dots as Förster Resonance Energy Transfer Agents for Diagnostics and Cellular Imaging

Daniel Geißler,[†] Stina Linden,[‡] Konstanze Liermann,[§] K. David Wegner,[‡] Loïc J. Charbonnière,[⊥] and Niko Hildebrandt*[,‡]

[†]BAM, Federal Institute for Materials Research and Testing, Division 1.10 Biophotonics, Berlin-Adlershof, Germany

[‡]NanoBioPhotonics, Institut d'Electronique Fondamentale, Université Paris-Sud, Orsay, France

[§]NanoPolyPhotonics, Fraunhofer Institute for Applied Polymer Research, Potsdam-Golm, Germany

[⊥]Laboratoire d'Ingénierie Moléculaire Appliquée à l'Analyse, IPHC, UMR 7178 CNRS-Université de Strasbourg, ECPM, Strasbourg, France

Supporting Information

ABSTRACT: Luminescent lanthanide labels (LLLs) and semiconductor quantum dots (QDs) are two very special classes of (at least partially) inorganic fluorophores, which provide unique properties for Förster resonance energy transfer (FRET). FRET is an energy-transfer process between an excited donor fluorophore and a ground-state acceptor fluorophore in close proximity (approximately 1−20 nm), and therefore it is extremely well suited for biosensing applications in optical spectroscopy and microscopy. Within this cogent review, we will outline the main photophysical advantages of LLLs and QDs and their special properties for FRET. We will then focus on some recent applications from the FRET biosensing literature using LLLs as donors and QDs as donors and acceptors in combination with several other fluorophores. Recent examples of combining LLLs and QDs for spectral and temporal multiplexing from single-step to multistep FRET demonstrate the versatile and powerful biosensing capabilities of this unique FRET pair. As this review is published in the Forum on Imaging and Sensing, we will also present some new results of our groups concerning LLL-based time-gated cellular imaging with optically trifunctional antibodies and LLL-to-QD FRET-based homogeneous sandwich immunoassays for the detection of carcinoembryonic antigen.

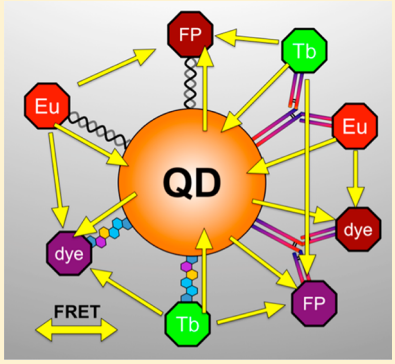

INTRODUCTION

Although the discovery of nonradiative energy transfer between two molecules at distances beyond orbital overlap and below radiative-transfer interactions dates back to the beginning of the 20th century,[1] the main contributions of Theodor Förster were published in the late 1940s,[2−4] and after Stryer and Haugland's famous paper "Energy Transfer: A Spectroscopic Ruler" appeared in 1967,[5] the application of Förster resonance energy transfer (FRET) underwent an enormous increase in the last 20 years (cf. Figure S1 in the Supporting Information, SI). This growing interest in FRET is based on the nanometric distance range of the FRET donor−acceptor interaction and the appearance of many new donor−acceptor pairs. The need for analyzing and utilizing new biological systems and interactions at distances of a few nanometers, the development of nanoparticles, fluorescent proteins, and many other new types of fluorophores and the impressive advancement of light excitation and detection technologies have fostered the frequent application of FRET.[6−15] The large majority of FRET publications can be found in the research areas of biochemistry, molecular biology, and chemistry (cf. Table S1 in the SI), where imaging and sensing of interactions, distances, and concentrations play an important role. Many books and review articles have been published about FRET, and a comprehensive book purely dedicated to FRET, including theory, technical background, and many different applications, has just appeared in 2013.[16]

In this review, we will focus on two very special inorganic FRET agents, namely, luminescent lanthanide labels (LLLs) and semiconductor quantum dots (QDs). Both of these fluorophores already provide unique photophysical properties on their own. The most important ones are the extremely long excited-state lifetimes (up to several milliseconds) for LLLs and color tunability combined with large and spectrally broad molar absorptivity for QDs. The combination of LLL donors with QD acceptors for FRET adds another important requirement, which is the possibility of energy transfer over very large distances. LLL−QD FRET pairs can enlarge the often-cited FRET distance range of 1−10 nm to ca. 20 nm because they are able to provide Förster distances (the donor−acceptor distance of 50% FRET efficiency), which are already larger than 10 nm.[17] Since our last microreview about LLL-to-QD FRET in

Special Issue: Imaging and Sensing

Received: July 11, 2013
Published: October 7, 2013

dx.doi.org/10.1021/ic4017883 | Inorg. Chem. 2014, 53, 1824−1838

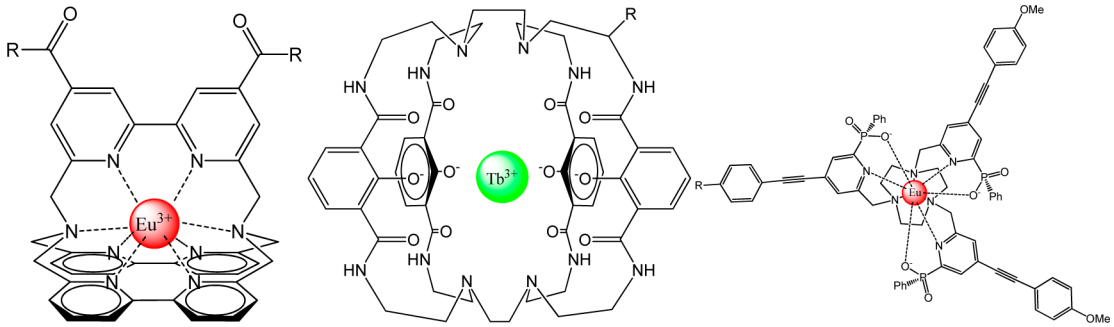

Figure 1. Representative examples of LLLs (R stands for the place of introduction of the activated function).[30,31,36,37]

2008,[18] many new developments, such as ultrasensitive multiplexing and FRET relays, have been realized, and large progress has been made in fluorescence imaging using LLLs and QDs. We will first outline some theory and technical background concerning LLLs, QDs, and FRET and will then focus on recent applications in diagnostics and cellular imaging. The application section also contains some of our latest and new results concerning terbium-based time-gated (TG) FRET cellular imaging using an optically trifunctional antibody and Tb-to-QD FRET-based in vitro diagnostics for the sensitive homogeneous detection of carcinoembryonic antigen (CEA).

THEORY AND TECHNICAL BACKGROUND

LLLs. Because of their long-lived excited states, LLLs are playing a particular role in the pool of luminescent compounds (usually called fluorophores, although luminophores would be the correct term in order to include other than singlet−singlet transitions). After a pulsed excitation of lanthanide complexes, the decay of the excited state to the ground state can be as long as a few milliseconds, while conventional fluorophores do not last more than a few tens of nanoseconds in their excited states before decaying. This large (ca. 1 million-fold) temporal difference makes time-resolved acquisition of the luminescent signal arising from LLLs a particularly sensitive technique.[19,20]

The detailed properties of luminescent lanthanide complexes have been described in numerous excellent review articles,[21−27] and we will only briefly recall them. LLLs are composed of an emitting lanthanide (Ln) cation (for most of them Tb^{3+} and Eu^{3+}) coordinated by an aromatic ligand, which serves both as a photon-collecting antenna and as a protective shield toward solvent molecules, competing anions, and coordinating molecules. To assume its protecting rule, the ligand generally provides a high denticity (Ln^{3+} cations generally exhibit coordination numbers of 8−10 in aqueous solutions), and it contains hard Lewis base functionalities such as acetates, phosphonates, or phosphinates, or a macropolycyclic framework, to provide the complex with high thermodynamic stability and kinetic inertness, sine qua non conditions to its efficiency in biological media. Because of the indirect excitation of the Ln ion of interest through the coordinated ligand, the excitation and emission wavelengths of the complexes are at significantly different energy levels, pointing to an abusively called "large Stokes shift". The emission spectra of LLLs are dominated by the f−f transitions of the Ln cations, which are faintly perturbed by the surrounding medium, affording a spectral signature typical for each lanthanide. Last but not least, the binding of LLLs to biological material requires the introduction of an activated function into the ligand backbone that will allow the strong covalent bonding necessary for biochemical analysis.[28,29] Similar to their fluorescent analogues, the efficiency of LLLs can be quantified by their brightness, which can be defined as a product of the molar absorptivity (generally the molar extinction coefficient at maximum excitation of the complex) and overall photoluminescence quantum yield.

The pioneering work in the field has been mainly directed toward europium complexes, in particular through the development of the family of [Eu(TBP)] complexes (TBP = tris-bipyridine) by Lehn and co-workers (Figure 1, left).[30,31] Although the TBP ligand affords a good photosensitization of the Eu^{3+} cation, it does not completely fulfill the first coordination sphere of the metal, leaving space for water molecules. Numerous fluoroimmunoassays using [Eu(TBP)] as the energy donor require the use of large amounts of NaF or KF because fluoride ions bind to the free coordination site to keep away water molecules, which cause quenching of lanthanide luminescence.

Despite some intrinsically better photophysical properties such as longer excited-state lifetimes or their multiplexing capabilities,[17] efficient terbium labels emerged only more recently at the beginning of this century.[32−35] One of the most relevant examples is the macrocyclic ligand developed by Raymond and co-workers (Figure 1, middle).[36] Thanks to four 2-hydroxyisophthalamide moieties, the maximum of absorption was observed at ca. 340 nm, close to the visible domain, with a noticeable brightness of 12636 M^{-1} cm^{-1} in a buffered aqueous solution. The terbium complex can be conjugated to biomolecules and has already proven to be a very efficient energy donor in time-resolved FRET experiments.

Very recently, there has been a renewed interest toward europium complexes carrying electron-donating functionalized pyridines and picolinic acids.[38,39] Parker and co-workers have taken advantage of the preorganization around a triazacyclononane framework to introduce three such antennae around a Eu^{3+} cation (Figure 1, right).[37] The excitation maximum is found at 332 nm, and the very large absorption of each unit afforded an excellent brightness of ca. 32400 M^{-1} cm^{-1}, thereby establishing it as one of the brightest LLLs. Although the presented work only refers to cellular staining, pointing to a good chemical stability in living organisms, it is worth noting that the introduction of labeling functions has already been studied[40] and will most probably appear in the literature in the near future.

The development of ever-more-performing LLLs [including lanthanide-doped nanoparticles (Ln-NPs) and up-converting nanophosphors (UC-NPs), which are briefly mentioned in the applications section below] keeps attracting the interest of chemists and will undoubtedly lead to new perspectives for

dx.doi.org/10.1021/ic4017883 | Inorg. Chem. 2014, 53, 1824−1838

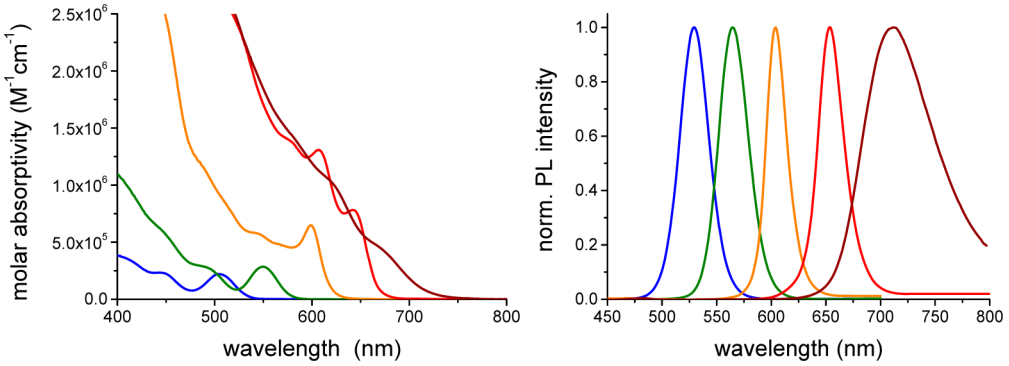

Figure 2. Typical absorption (left) and emission spectra (right) of different-sized semiconductor QDs revealing their large absorption cross sections with high extinction coefficients (>1 × 10^6 M^{-1} cm^{-1}) increasing toward UV and their narrow and symmetric emission bands enabling multiplexed detection of different QDs in the same sample. Blue, green, orange, and red are CdSe/ZnS core/shell QDs, whereas brown is a CdSeTe/ZnS core/shell QD.

FRET applications in the fields of multiplexed analysis, relayed FRET, and possibly energy-transfer processes in the near-IR (NIR) region.

Semiconductor QDs. QDs are luminescent colloidal nanocrystals that display unique optical (and electronic) properties resulting from their semiconductor material characteristics and their nanometer sizes that lead to quantum confinement effects.[41−43] QDs are composed of semiconductor cores, which are often coated with one or more shell(s) consisting of another semiconductor material with suitable lattice parameters and a higher band-gap energy (for type I QDs, e.g., CdSe/ZnS core/shell or CdSe/CdS/ZnS core/shell/shell QDs). The shell passivates the QD core from quenching effects because of surface defects (leading to so-called trap states) and the surrounding medium, thus increasing the photoluminescence quantum yields of (type I) QDs.[41,43−47]

In order to create stable, water-soluble, and biocompatible QDs, several different synthetic strategies have been developed within the last 20 years. These strategies include (a) exchange of the hydrophobic ligands with ligands containing one or more thiol groups on one side and (hydrophilic) carboxyl groups on the other (e.g., thioglycolic acid, mercaptopropionic acid, dihydrolipoic acid, or cysteine), (b) ligand modification to turn the hydrophobic surface ligands into hydrophilic ones, (c) surface capping with amphiphilic molecules or comblike (coblock) polymers possessing a hydrophilic backbone and hydrophobic side chains, (d) coating with water-soluble polymers or PEGylated ligands, or (e) silanization to encapsulate the hydrophobic QD within a hydrophilic silica shell.[46−52] Apart from the hot injection method, other QD synthesis techniques (bottom-up as well as top-down) have been developed; for instance, some QDs can be synthesized directly in water using either laser ablation or special water-soluble precursor materials.[53,54]

In addition to the phase-transfer concepts mentioned above, various surface functionalization methods for attaching oligonucleotides (DNA or RNA), peptides, proteins, and other biomolecules to QD surfaces were developed. These methods include (a) the direct attachment of thiol- or His-tag-containing molecules onto the QD surface (self-assembly), (b) electrostatic interaction between the biomolecule (e.g., peptides) and the surface ligands, (c) covalent binding to reactive groups of the surface ligands or polymer coatings using EDC/NHS chemistry, heterobifunctional cross-linkers (e.g., SMCC), click chemistry, or bioorthogonal chemistry concepts, and (d) secondary interactions such as biotin−streptavidin binding.[46,49,55,56]

The photophysical properties of QDs can be controlled by their nanocrystal core sizes, the shell thickness(es), and the composition of the semiconductor materials of cores and shell(s) and partly by their surface ligands. Thus, the final absorption and emission features of QDs can be tuned from UV to NIR to fit the desired spectral characteristics, making them ideally suited for all kinds of spectroscopic applications. QDs can have extremely high molar absorptivities (extinction coefficients) of more than 1 × 10^6 M^{-1} cm^{-1} over broad wavelength ranges, showing an onset at their first exciton peak (lowest energy needed to excite the QD by creating an electron−hole pair) and a continuous increase toward UV (Figure 2, left). In contrast, QDs display narrow and symmetric, nearly Gaussian-shaped emission bands (Figure 2, right) characteristic for their size-dependent band-gap energy. QDs can be excited far below their emission wavelengths, enabling an easy discrimination of the excitation and emission signals using short- and/or long-pass filters. Moreover, several different-sized (and therefore different-colored) QDs can be excited at the same wavelength using a single excitation source. This, in combination with their narrow and symmetric emission bands, allows the use of multiple QDs in the same sample (multiplexing) with an efficient spectral discrimination of their emission signals.[17,52,57−60]

In addition to their size-dependent absorption and emission bands, QDs are highly photostable compared to common organic dyes (highly reduced photobleaching) and they often provide high photoluminescence quantum yields, even in the NIR region.[47−49,52,61] Because of their outstanding photophysical properties, QDs are suited for a wide range of applications in the fields of optics and optoelectronics (e.g., lasers and displays[62,63]) and photovoltaics (e.g., solar energy harvesting and conversion[62,64,65]) and as labels and sensors in biochemistry, biotechnology, and medicine (e.g., fluorescence spectroscopy and microscopy[47,48,52,66−68] as well as FRET-based assays and diagnostics[69]). There are persisting concerns about the toxic effects of QDs, and a general statement concerning QD toxicity cannot be made because different types of QDs show different toxic effects.[70,71] Recently, it was shown that QD toxicity (impact on cellular proliferation) is similar to the toxicity of various commercial cell-labeling fluorophores.[72] Thus, the choice of the right fluorophore (dye, fluorescent protein, QD, etc.) should be based on the application.

dx.doi.org/10.1021/ic4017883 | Inorg. Chem. 2014, 53, 1824−1838

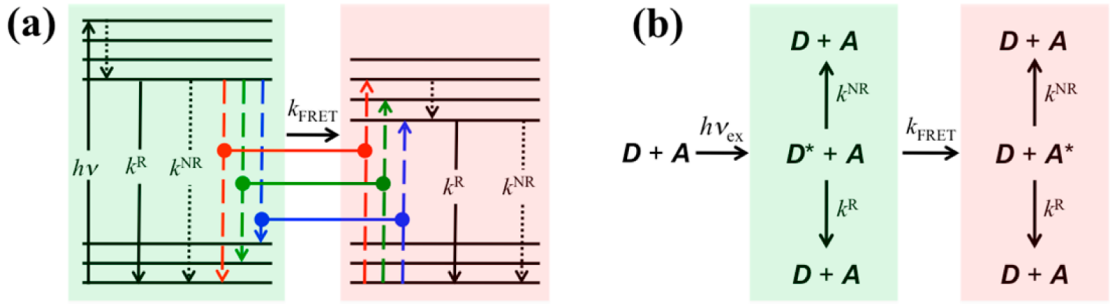

Figure 3. Principle of donor (green background) and acceptor (red background) interaction in FRET. (a) Simplified energy-level diagram representing excitation of the donor ($h\nu$) followed by inner relaxation (dotted arrow), followed by radiative decay (k^R), nonradiative decay (k^{NR}), or FRET (k_{FRET}). The energy resonance condition [ΔE(donor) = ΔE(acceptor)] is represented by the colored lines connecting donor and acceptor transitions. After FRET, the acceptor is in an excited state, followed by radiative or nonradiative decay to its ground state. (b) Different energy pathways after donor excitation ($h\nu_{ex}$) leading to radiative (k^R) or nonradiative (k^{NR}) decay of the donor or acceptor in case it is excited by FRET (k_{FRET}). D, D* and A, A* indicate the ground or excited state of the donor and acceptor, respectively.

FRET. Theory and applications of FRET have been reviewed in detail elsewhere,[6,7,9−15,73,74] and here we will focus on the essential concepts and most important basics. FRET describes a nonradiative energy transfer between a luminescent donor and a light-absorbing acceptor. The luminescence energy (in spectroscopy and imaging usually expressed in wavelength) of the donor must be equal to the absorption energy (wavelength) of the acceptor, which is the so-called *resonance condition* (*resonance* energy transfer; cf. Figure 3a). FRET is based on the approximation that dipole−dipole coupling can be represented by Coulombic coupling, which is coupling of the transition dipole moments of donor emission and acceptor absorption. Coulombic coupling should be dominant at a FRET distance range of ca. 1−20 nm, where orbital-overlap-related mechanisms (for very short distances) and radiative mechanisms (for long distances) play minor roles. The FRET efficiency η_{FRET} is dependent on the donor−acceptor distance r ($\eta_{FRET} \sim r^{-6}$). η_{FRET} is 50% when the FRET rate k_{FRET} and all other decay rates (radiative and nonradiative deactivation defined by the rates k^R and k^{NR}, respectively) are in equilibrium ($k_{FRET} = k_D^R + k_D^{NR} = \tau_D^{-1}$). The distance ($r = R_0$) for this case is called the Förster distance (or Förster radius) and is defined by eq 1.

$$R_0 = \left(\frac{9(\ln 10)\kappa^2 \Phi_D}{128\pi^5 N_A n^4} J \right)^{1/6} \tag{1}$$

Here κ^2 is the orientation factor between the two transition dipole moments, Φ_D is the donor luminescence quantum yield, N_A is Avogadro's number, n is the refractive index of the surrounding medium (usually the solvent), τ_D is the donor luminescence lifetime (in the absence of the acceptor), and J is the spectral overlap integral [defined on the wavelength (λ) or wavenumber ($\tilde{\nu}$) scale] defined by eq 2.

$$J = \int \bar{I}_D(\lambda)\, \varepsilon_A(\lambda)\, \lambda^4\, d\lambda = \int \bar{I}_D(\tilde{\nu})\, \varepsilon_A(\tilde{\nu})\, \frac{d\tilde{\nu}}{\tilde{\nu}^4} \tag{2}$$

J is dependent on the acceptor molar absorptivity (or extinction coefficient) spectrum ε_A and the donor area-normalized emission spectrum $\bar{I}_D$ (the integral of $\bar{I}_D$ is unity). In the case where J is calculated in $M^{-1}\ cm^{-1}\ nm^4$, the Förster distance can be calculated using eq 3.

$$R_0 = 0.02108(\kappa^2 \Phi_D n^{-4} J)^{1/6}\ \text{nm} \tag{3}$$

After donor excitation, FRET deactivation is in competition with radiative and nonradiative deactivation of the donor. In case the acceptor gets FRET-sensitized, it can again return to its energetic ground state by radiative or nonradiative transitions (cf. Figure 3b).

The FRET efficiency can be calculated using distances or spectroscopic data [eq 4 with luminescence quantum yields Φ, decay times τ, or intensities I of the donor in the absence (subscript D) and presence (subscript DA) of the acceptor, respectively].

$$\eta_{FRET} = \frac{1}{1 + \left(\frac{r}{R_0}\right)^6} = \frac{{R_0}^6}{{R_0}^6 + r^6} = 1 - \frac{\Phi_{DA}}{\Phi_D}$$
$$= 1 - \frac{\tau_{DA}}{\tau_D} = 1 - \frac{I_{DA}}{I_D} \tag{4}$$

Equation 4 also allows calculation of the donor−acceptor distances by spectroscopic data (spectroscopic ruler). η_{FRET} can be sensitively measured at donor−acceptor distances between ca. $0.5R_0$ and $2.0R_0$ (Figure S2 in the SI).

Another important variable for FRET is the orientation factor (κ^2). Depending on the orientation between the transition dipole moments of the donor and acceptor, κ^2 can take values between 0 (perpendicular orientation) and 4 (head-to-tail parallel orientation). However, there are some reasonable averaging conditions. When the average rotation rate of donors and acceptors is much larger than the average FRET rate, the system is in a dynamic averaging regime and κ^2 becomes $^2/_3$. Fast isotropic rotation can, e.g., be verified by unpolarized emission. If one of the FRET partners shows average orientation and the other has a fixed orientation, κ^2 can take values between $^1/_3$ and $^4/_3$. In the case where all donors and acceptors are fixed (no rotational motion), each FRET pair is assumed to be isolated from all other pairs, and the electronic transitions are single dipoles, one can use a static regime approximation,[73] for which κ^2 is dependent on r and can take values between 0 (for very short distances) and $^2/_3$ (for very large distances). Detailed studies of κ^2 can be found in refs 75 and 76.

There are various possibilities to detect FRET. Steady-state (SS) and/or time-resolved spectroscopy and microscopy can be applied for determination of the FRET efficiencies and distances using donor quenching, acceptor sensitization, combined donor quenching and acceptor sensitization, donor photobleaching, or acceptor photobleaching. The almost endless choice of donor−acceptor combinations and the use

dx.doi.org/10.1021/ic4017883 | Inorg. Chem. 2014, 53, 1824−1838

of multiple donors and/or acceptors allow further flexibility in order to find and optimize a FRET system for many different applications.

LLLs as FRET Donors. Although lanthanides have also been used as FRET acceptors,[77,78] the advantages of LLLs are mainly used for their application as FRET donors.[8,14,79] The main benefit is their long luminescence decay of up to a few milliseconds,[25,26,80,81] which is several orders of magnitude longer than the decay times of any acceptor (usually in the nanosecond range). This large difference in the donor and acceptor excited-state lifetimes leads to approximately equal luminescence decay behaviors of the donor and acceptor in case the acceptor is excited by FRET via the donor. This means that the decay time of the donor in the presence of the acceptor (τ_{DA}) equals the one of the acceptor in the presence of the donor ($\tau_{AD} = \tau_{DA}$).[74] The big advantage of this equality is that the same decay time analysis can be applied for donor quenching and acceptor sensitization. This gives two independent detection channels for FRET (the donor behavior can be verified by the acceptor behavior), with the acceptor channel being the "FRET-proof" channel, because the acceptor emission can only be caused by excitation via FRET. The much longer excited states also allow FRET from multiple LLLs to a single acceptor. The short excited-state lifetime of the acceptor will lead to almost immediate deexcitation after FRET so that the same acceptor can be FRET-sensitized again by another LLL donor, which is still in the excited state. This effect will not increase the FRET efficiency per donor (it might even decrease because several donors are in competition for a single acceptor), but it will increase the overall brightness per acceptor, which can lead to higher sensitivities for such multiple-LLL-donors/single-acceptor FRET systems. The acceptor emission can be measured against a very low background if the acceptor emits at a wavelength region without lanthanide emission, as depicted in Figure 4 for terbium. Although for FRET these emission wavelengths must be longer than the first emission peak of the lanthanide emission spectrum, energy transfer from lanthanides to acceptors with shorter emission wavelengths has been found.[82,83] Because this energy transfer is not based on spectral overlap, the authors named the phenomenon "nonoverlapping FRET" (or nFRET). Although a detailed study of nFRET is not available, their results indicated that energy transfer most probably occurs from higher energy levels of the lanthanide (europium and samarium in their cases), which do not participate in emission, and therefore no overlap of donor emission and acceptor absorption is required. The selection of the appropriate acceptor can be made from a large variety of fluorophores (e.g., fluorescent proteins, organic dyes, QDs).[11,84−86] Fluorescence background of the sample matrix (sample autofluorescence) and of directly excited acceptors, which are usually in the nano- to microsecond time range, can be efficiently suppressed by pulsed excitation and detector gating (e.g., detection windows of 0.05−2 ms). This will lead to a pure FRET signal because TG photon detection will most probably arise from FRET-sensitized excitation. Because only complete donor−acceptor pairs can lead to FRET-sensitized TG acceptor emission signals, this method is insensitive to concentration effects and incomplete labeling and binding.

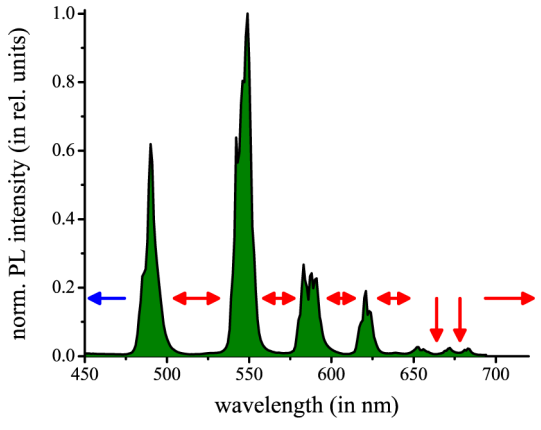

Figure 4. Well-separated emission lines of LLLs (in this case, a terbium photoluminescence spectrum is shown) allowing for a large choice of possible FRET acceptors, whose emission bands should be placed in LLL-free emission wavelength ranges (indicated by the red arrows) for the suppression of LLL background emission. The blue arrow indicates the wavelength range for nFRET acceptors (note that this has only been shown for europium and samarium and not for terbium).

Another advantage of using LLLs as FRET donors is the possibility of large overlap integrals and concomitant large Förster distances. This becomes possible when the LLL emission spectrum is entirely covered by an acceptor absorption spectrum with large molar absorptivity values. Förster distances of 9 nm for an europium-cryptate donor and an APC acceptor[87] and up to 11 nm for a terbium-chelate donor and QD acceptors[17] have been reported, which are much larger than R_0 values of conventional donor−acceptor pairs (values larger than 6 nm are rarely found).[88] One very comfortable aspect concerning the orientation factor κ^2 is the unpolarized emission of most lanthanide complexes. Their multiple transition dipole moments make them a randomized donor, and κ^2 gets limited to values between $^1/_3$ and $^4/_3$ even if the acceptor has a fixed orientation.

QDs as FRET Donors and Acceptors. QDs can be used as both FRET donors and acceptors, which have been treated in several comprehensive reviews in the recent literature.[49,69,89−91] As donors, QDs can be combined with a large variety of acceptors (e.g., organic dyes or fluorescent proteins). The main advantages of the QDs in the donor configuration are (i) their size tunability, which allows construction of an ideal spectral overlap with almost any acceptor, (ii) their broad absorption spectra, which allow excitation at almost any wavelength, preferably at a wavelength where the acceptor does not absorb, and (iii) the attachment of several acceptors to the relatively large QD surface (compared to small organic molecules), which allows an increase of the FRET efficiency with the number of acceptors (n):

$$\eta_{FRET} = \frac{nR_0^6}{nR_0^6 + r^6} \quad (5)$$

Using QDs as acceptors is less common because of their broad ecxitation spectra, which will cause QD excitation at almost any wavelength (independent of the donor). This will lead to many QD acceptors in excited states, which is very counterproductive for FRET (the acceptor must be in the ground state). Although energy transfer to QDs from other QDs,[92] organic dyes,[93] or UC-NPs has been described,[94] there are mainly two concepts to overcome the direct excitation limitation. The first one is to use LLLs as donors because their long excited states (milliseconds) will allow efficient FRET after all QDs have

dx.doi.org/10.1021/ic4017883 | Inorg. Chem. 2014, 53, 1824−1838

decayed back to their ground states (after nano- to microseconds).[17,95−99] The second one is to avoid any light ecxitation and to use bioluminescent or chemiluminescent donors.[100−103] Similar to that for the donor configuration, the main advantages of using QDs as acceptors are (i) their size tunability, which allows the use of several QD acceptors for the same donor without spectral crosstalk of their respective emission spectra, (ii) their large and spectrally broad molar absorptivities (extinction coefficients), which allow very large spectral overlap integrals and therefore long Förster distances, and (iii) the attachment of several donors to the relatively large QD surface, which can allow an efficient increase of the probability of QD FRET sensitization (but no increase of the FRET efficiency) with the number of donors. If sufficient excitation intensity is available for several donors and the QD is considered to be always in a ground state within the excited-state lifetime of the donors (which is a good approximation for LLL donors and a QD acceptor), the probability of QD FRET sensitization by m LLL donors can be approximated as

$$P = 1 - (1 - \eta_{\mathrm{FRET}})^m = 1 - \left(\frac{r^6}{R_0{}^6 + r^6}\right)^m \quad (6)$$

Equation 6 illustrates one of the advantages of LLL-to-QD FRET, which is a high overall brightness of the FRET system for multiple LLLs per QD (enhanced FRET-sensitized QD photoluminescence). Other benefits are very long Förster distances (>10 nm), low background emission (for TG detection), equal photoluminescence decay behavior ($\tau_{\mathrm{DA}} = \tau_{\mathrm{AD}}$), and excellent multiplexability (several different QDs as acceptors for the same type of LLL). All of these advantages make the LLL−QD donor−acceptor pair a very unique and powerful tool for many different FRET applications, as outlined in the following section.

RECENT APPLICATIONS OF LANTHANIDE- AND QD-BASED FRET

Because of their unique optical properties, LLLs and QDs are frequently used in various life science applications for fluorescence spectroscopy and microscopy with and without FRET. Here we give a short outline of recent FRET-based applications of LLL donors, QD acceptors, and their combination as a LLL−QD FRET pair and highlight a few representative examples from the literature and from our own latest research results concerning TG LLL-to-dye FRET imaging and LLL-to-QD FRET clinical diagnostics.

LLLs in FRET-Based Diagnostics. Luminescent lanthanide complexes, Ln-NPs, and UC-NPs are widely used in FRET-based biosensing because their long luminescence decay times enable highly sensitive, nearly background-free measurements by TG detection.[25,104,105] In most FRET diagnostic applications, terbium and europium complexes are utilized, but the use of Ln-NPs and UC-NPs has increased over the last years because they provide some further photophysical benefits. Within Ln-NPs, the lanthanide dopants are shielded against quenching effects of the surrounding medium without supramolecular "cages" as used for the chelate- or cryptate-based lanthanide complexes.[106] The main interest of UC-NPs is their efficient excitation in the NIR via two- or more-photon absorption and energy up-conversion processes, which further minimizes background signals arising from the scattering of incident light and autofluorescence due to direct sample excitation.[107,108]

LLLs have already been applied in numerous bioanalytical FRET experiments to monitor biological binding events (ligand−receptor or protein−protein interactions) and to detect biomarkers using in vitro assays,[8,21,25,81,104,109−115] to investigate conformational changes and molecular structures (spectroscopic or molecular ruler),[5,104,116−118] and to measure nucleic acid sequencing and hybridization assays.[119−121] Terbium and europium complexes are used in several commercial homogeneous TR-FRET assays, e.g., in clinical diagnostics for the detection of many different biomarkers (HTRF,[122] LANCE,[123] and TRACE). Recently, luminescent lanthanide complexes have been utilized for selective protein labeling and time-resolved bioassays,[124] for screening for protein−protein interactions and their inhibition,[125,126] and for detection of several analytes or parameters simultaneously within multiplexed FRET assays.[127−130] New applications of Ln-NP-based FRET biosensing include their use as donors with rhodamine B dye acceptors for intracellular FRET experiments,[131] with gold nanoparticle (AuNP) quenchers in a biotin−streptavidin affinity assay,[132] and with fluorescein isothiocyanate acceptors for avidin detection.[133] UC-NPs have been recently applied as FRET donors for organic dyes within a dual-parameter hybridization assay[134] and in combination with rhodamine 6G acceptors as luminescence temperature sensors.[135] In a proof-of-principle study, UC-NPs have also been used as FRET donors for QD acceptors.[94]

As mentioned above, LLL-based FRET is an established technology in clinical diagnostics. A very sensitive random-access immunoanalyzer system using mainly Eu-to-APC FRET (Tb-to-dye FRET is also used for some assay kits) within homogeneous sandwich immunoassays is the KRYPTOR fluorescence plate reader (Cezanne, BRAHMS, Thermo Fisher Scientific). The various immunoassay kits that exist for this reader system are already far beyond basic research on FRET or lanthanide complexes because they are used in daily in vitro diagnostic testing and large clinical studies. One important clinical example of such an "end user" application of LLL-based FRET diagnostics is the detection of the infection marker procalcitonin (PCT). In a recent clinical study by Shomali et al., the role of PCT in 248 nonneutropenic cancer patients (NNCPs) with fever was investigated using the Eu-to-APC FRET-based PCT KRYPTOR immunoassay kit with a limit of quantification of 0.075 ng/mL PCT.[136] Neutropenia is a disorder resulting in a decrease of white blood cells, which destroy bacteria in the blood and are thus a primary defense against infections. The diagnosis of NNCPs with fever of unknown origin is challenging because it may arise from malignant tumors. Therefore, the authors measured PCT in plasma samples from NNCPs with solid tumors, lymphoma, or multiple myeloma and fever (≥38 °C) within 1 and 4−7 days after fever onset. The obtained PCT levels were correlated with the patients' clinical, microbiological, and radiological data to differentiate infectious and noninfectious fever. The results showed that increased PCT levels are predictors of bloodstream infection (median [PCT] = 1.06 ng/mL) and sepsis (median [PCT] = 0.60 ng/mL) in NNCPs (median [PCT] = 0.31 ng/mL for patients with no documented infection). PCT levels may also be predictors of metastasis (0.47 vs 0.20 ng/mL without metastasis) and advanced cancer (0.47 ng/mL for stage IV cancer vs 0.27 ng/mL for stage I−III cancer). The relationship between the PCT levels and the patients' response to antibiotic treatment could be monitored by a decrease of the median PCT concentration from 0.52 ng/mL (before antibiotic

dx.doi.org/10.1021/ic4017883 | Inorg. Chem. 2014, 53, 1824−1838

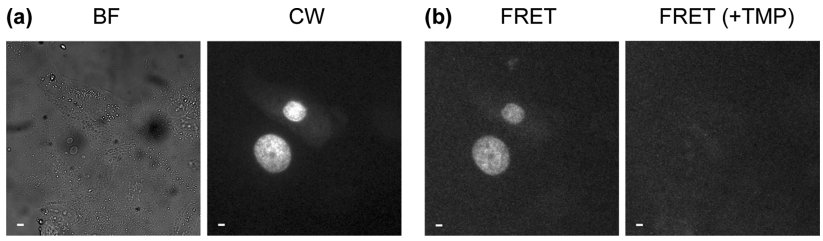

Figure 5. (a) Bright-field (BF; left) and continuous-wave (CW; right) fluorescence (λ_{exc} = 545 ± 15 nm; λ_{em} = 610 ± 35 nm) images of MDCKII cells expressing H2B-TagRFPT-eDHFR after incubation with TbL4-TMP-CPP. The SS (CW) fluorescence image shows that the fluorescent TagRFPT proteins are localized in the cell nulcei. (b) TG FRET images (delay = 10 μs; λ_{exc} = 365 nm; λ_{em} = 605 ± 7 nm) before (left) and after (right) the addition of 100 μM TMP. Before TMP addition, FRET signals from the nuclei are observed because of long-lived terbium-sensitized TagRFPT acceptor emission, whereas the FRET signals vanish after TMP addition because the TbL4-TMP conjugates are replaced from the eDHFR binding sites by pure TMP. Reproduced with permission from ref 142. Copyright 2012 Wiley-VCH.

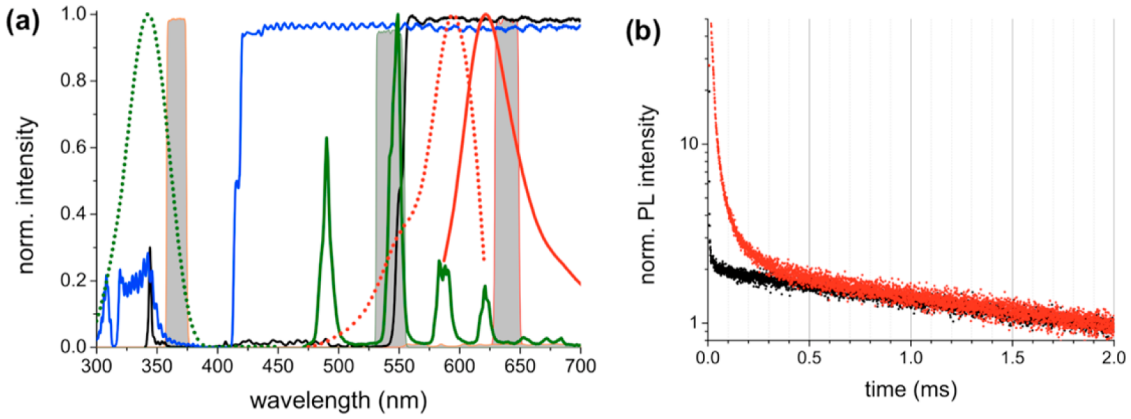

Figure 6. (a) Intensity normalized excitation (dotted lines) and emission (solid lines) spectra of TbL4 (green) and AF594 (red) and transmission spectra of the band-pass filters (365 nm, orange; 542 nm, green; 640 nm, red; all with gray background) and dichroic mirrors (405 nm, blue; 552 nm, black) used in the imaging setup. (b) Photoluminescence (PL; normalized to the PL intensity at 2.0 ms) decay curves of pure TbL4 (black) and TbL4–AF594 antibodies (red) both excited at 349 nm and detected at 490 and 636 nm for TbL4 and AF594, respectively. *Note: This is new and so-far-unpublished data.*

treatment) to 0.19 ng/mL (after 4–7 days with antibiotic treatment). The decreased follow-up PCT levels upon antibiotic treatment, allowing one to differentiate infectious fever from tumor-related fever, may lead to a more efficient use of antibiotics and thus reduce the therapy duration, emergence of resistance, and costs. The use of the LLL-FRET-based immunoassay technology in such clinical studies demonstrates the high sensitivity (sub-ng/mL detection) and degree of automation that is necessary for high-performance diagnostic tests that need to be performed by persons without expertise in spectroscopy or FRET.

LLLs in FRET-Based Imaging. Despite their broad application in spectroscopic biosensing, LLLs have been much less used as FRET agents in cellular imaging.[96,137−140] This is mainly caused by the unconventional equipment for TG imaging, which is necessary to profit from efficient background suppression by taking advantage of the long luminescence decay times of LLLs. Intensified CCD (ICCD) cameras and pulsed excitation sources are required to achieve time gating on the micro- to millisecond time scale. Much recent work concerning TG FRET imaging with terbium complexes has been realized in the group of Miller.[141,142] The excitation/emission principle uses a UV-emitting light-emitting diode (LED; 365 nm), which excites the terbium complex during ca. 1.5 ms. After that excitation period, the LED is switched off, and after a delay of ca. 10 μs, the ICCD detector is switched on for approximately 1.5 ms for measuring the TG emission intensity of terbium and/or an acceptor fluorophore (sensitized by the terbium donors).[141]

This technique was applied in 2012 by Mohandessi et al. to cellular imaging using cell-penetrating peptides (CPPs) as delivery vehicles for the luminescent terbium complex Lumi4-Tb (TbL4, Lumiphore) and heterodimers of Lumi4-Tb and a derivative of trimethoprim (TbL4-TMP).[142] The applied CPPs, including nona-arginine (Arg_9) and HIV Tat-derived sequences (Tat), were covalently bound to the terbium complexes and mediated the passive delivery of the otherwise cell-impermeable TbL4 and TbL4-TMP to the cytoplasm of various cell types (e.g., Maden Darby canine kidney epithelial cells, MDCKII). The authors applied TG microscopy to visualize the successful peptide delivery and subcellular distribution. The TG images revealed located terbium luminescence at low peptide concentrations (due to endocytosis) but a diffuse distribution of the terbium luminescence throughout the cytoplasm and nucleus at peptide concentrations higher than 20–60 μM, suggesting direct translocation of the CPP conjugates from the cell culture medium to the cytoplasm and free diffusion throughout the cytoplasm and nuclei. In order to demonstrate specific labeling of the intracellular TbL4-TMP-CPP conjugates to *Escherichia coli* dihydrofolate reductase (eDHFR) fusion proteins in live cells, the authors used FRET from TbL4 to the red fluorescent protein TagRFPT. MDCKII cells were transfected with DNA that encodes a three-component protein chimera of histone 2B (H2B), TagRFPT, and eDHFR. After

dx.doi.org/10.1021/ic4017883 | *Inorg. Chem.* 2014, 53, 1824−1838

incubation with TbL4-TMP-CPP, Tb-to-TagRFPT FRET was observed by TG imaging, demonstrating the binding of TbL4-TMP to eDHFR within the cell nuclei after CPP-mediated delivery. Colocalization of TbL4 and TagRFPT (or TMP and eDHFR) was verified by SS emission of TagRFPT upon direct excitation of TagRFTP (Figure 5a, right) and TG FRET-sensitized emission of TagRFPT upon excitation of TbL4 (Figure 5b, left), both measured at a wavelength of strong TagRFTP and very low terbium emission (605 nm; cf. Figure 4). The addition of 100 μM unconjugated TMP resulted in the complete disappearance of the long-lived FRET-sensitized TagRFTP emission because of replacement of TbL4-TMP (by an excess of pure TMP) from the TagRFTP expressing eDHFR constructs (Figure 5b, right). This demonstrated the previous attachment of TbL4-TMP to the H2B-TagRFPT-eDHFR protein chimera.

Apart from Miller's work, our groups have also investigated TG FRET imaging using LLLs as FRET donors in combination with different acceptor fluorophores. In an initial study, we demonstrated FRET from terbium complexes to QDs after pulsed UV-flash-lamp excitation.[96] The terbium-based LLLs were coupled to streptavidin (Tb-sAv), and Tb-sAv aggregates were incubated with biotinylated QDs. After time delays from 50 to 170 μs (when the luminescence of directly excited QDs has already vanished), TG QD emission could still be observed because of FRET sensitization by Tb-LLLs.

In the following paragraphs, we present some new data concerning Tb-to-dye FRET-based imaging for biosensing. We designed trifunctional luminescent antibodies that were labeled with both organic dyes and terbium complexes (on the same antibody). For this purpose, we used commercial goat antirabbit IgG antibodies labeled with Alexa Fluor 594 (AF594; Life Technologies) for cellular staining (against cellular marker-specific rabbit IgGs). We colabeled these antibodies with TbL4-NHS in order to design a TbL4–AF594 FRET pair on the same antibody. The strong spectral overlap of TbL4 emission and AF594 absorption (cf. Figure 6a) allows efficient FRET from TbL4 to AF594 so that either SS AF594 excitation and emission detection (detection mode 1), pulsed TbL4 excitation and TG terbium emission detection (detection mode 2), or pulsed TbL4 excitation and TG AF594 emission detection (detection mode 3) can be used for one single type of antibody.

Figure 6a shows the excitation and emission spectra of TbL4 and AF594 as well as the transmission spectra of the different applied dichroic mirrors and filters used for the different detection modes. Because multiple TbL4 donors and AF594 acceptors are randomly labeled over the antibody, they are in relatively close distance to each other and energy transfer is quite efficient (because of the multiple labeling, an exact distance cannot be estimated or measured), which can be seen in the luminescence decay curves in Figure 6b. Because of a strong emission signal of unquenched TbL4, arising mainly from free TbL4 in the TbL4–AF594 antibody solution, the FRET-quenched decay component is less visible in the terbium donor detection channel (not shown) compared to the AF594 acceptor detection channel, which contains relatively little terbium background emission. A comparison of the luminescence decays of pure TbL4 (black curve) and TbL4–AF594 antibodies (red curve) clearly shows the different contributions of terbium emission (long-lived tail visible in both curves) and FRET-sensitized AF594 emission (shorter decay in the first 0.5 ms in the red curve), which is significantly longer than emission from directly excited (no FRET) AF594 (in the nanosecond range). In order to demonstrate the use of the optically trifunctional antibodies in cellular imaging, we incubated PDGFR-β-expressing BJ-hTERT cells with anti-PDGFR-β rabbit primary IgGs. The fixed cells were then incubated with the goat antirabbit TbL4–AF594 IgG antibodies and washed of free TbL4 and TbL4–AF594 antibodies that were not able to bind to the primary IgGs. We then imaged the TbL4–AF594 antibody as well as the original AF594 antibody (no colabeling with TbL4) stained cells in the three detection modes: (1) CW excitation (542 nm) of AF594 and SS emission detection of AF594 (640 nm); (2) pulsed excitation (100 Hz, 349 nm) of TbL4 and TG detection (0.01–2.01 ms) of TbL4 (542 nm); (3) pulsed excitation (100 Hz, 349 nm) of TbL4 and TG detection (0.01–2.01 ms) of AF594 (640 nm). The obtained images (Figure 7) contain much interesting information. The

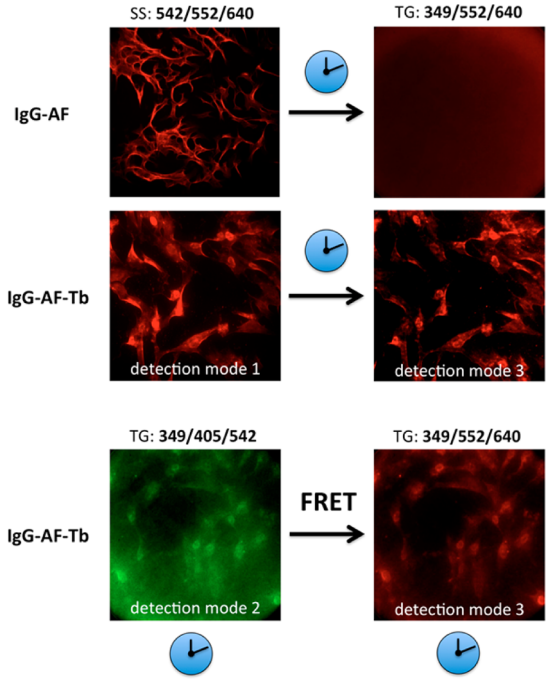

Figure 7. SS and TG (or clock symbol) imaging of BJ-hTERT cells stained with AF594 (top) and TbL4–AF594 antibodies (center and bottom). The different detection modes are (1) CW excitation of AF594 (542 nm) and SS emission detection of AF594 (640 nm); (2) pulsed excitation (100 Hz, 349 nm) of TbL4 and TG detection (0.01–2.01 ms) of TbL4 (542 nm); (3) pulsed excitation (100 Hz, 349 nm) of TbL4 and TG detection (0.01–2.01 ms) of AF594 (640 nm). Wavelengths (nm) of excitation (band-pass filter), splitting of excitation and emission (dichroic mirror), and emission (band-pass filters) are given on top of the images (excitation/splitting/emission). *Note: This is new and so-far-unpublished data.*

control samples (staining with AF594 antibodies only; IgG-AF in Figure 7) show that the AF594 emission signal, which is clearly visible at SS detection completely disappears when TG detection and UV excitation are used because AF594 is not efficiently excited and time gating from 0.01 to 2.01 ms is far beyond the luminescence decay time of AF594. The TbL4–AF594 stained cells (IgG-AF-Tb in Figure 7) also show a clear AF594 emission signal in detection mode 1. However, in contrast to the control samples, AF594 emission is also clearly visible in the TG detection mode 3, which demonstrates FRET sensitization of AF594 by TbL4 on the antibodies. It should be

dx.doi.org/10.1021/ic4017883 | *Inorg. Chem.* 2014, 53, 1824–1838

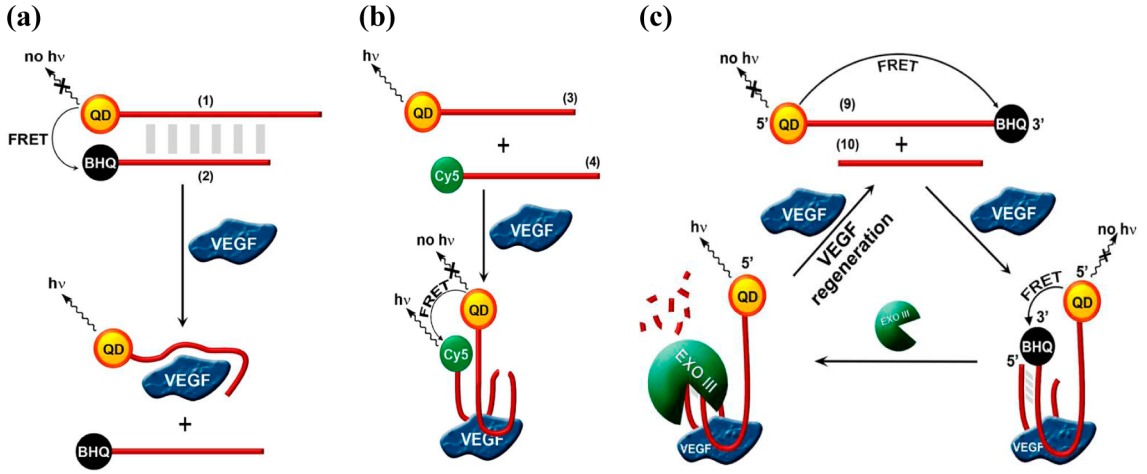

Figure 8. Schematic representations of different FRET-based aptasensors for detection of VEGF. (a) FRET aptasensor involving the VEGF-induced separation of aptamer-functionalized QDs initially blocked by black hole quencher (BHQ)-labeled complementary strands. In the absence of VEGF, both DNA strands are hybridized and QD luminescence is quenched via FRET. Upon the addition of VEGF, both strands are separated and 620 nm QD emission appears (LOD = 1 nM). (b) FRET-based aptasensor applying the VEGF-induced assembly of anti-VEGF aptamer subunits labeled with QD donors and Cy5 dye acceptors, respectively. In the presence of VEGF, both subunits bind to the analyte and QD-to-Cy5 FRET is observed (LOD = 12 nM). (c) Amplified FRET-based aptasensor utilizing Exo III to recycle the VEGF analyte. Here, the anti-VEGF aptamer subunits are labeled with QDs and BHQs, respectively, and QD luminescence is quenched initially. The addition of VEGF leads to partial hybridization of both subunits, resulting in digestion of the quencher-containing units by Exo III, releasing the VEGF analyte and switching on QD luminescence (LOD = 5 pM). Reproduced with permission from ref 168. Copyright 2012 American Chemical Society.

noted that part of the antibodies have lost their specificity toward the primary IgG because the cells appear completely stained whereas the control cells show specific membrane staining. However, this behavior was not important for demonstration of the three detection modes for the TbL4–AF594 antibodies. Using both TG detection modes 2 and 3 shows that both TbL4 and AF594 can be detected within the same cells after pulsed excitation of TbL4 in UV. The images also show a reduced background in the AF594 acceptor image (bottom right) compared to the TbL4 donor image (bottom left) because the signal in the AF594 channel can only arise from FRET-sensitized AF594 emission and not from unquenched TbL4 emission, as is still present in detection mode 2. In control experiments (Figure S3 in the SI), we showed that UV excitation of TbL4 inside cells does not lead to any significant Tb emission background signal beyond 630 nm (beyond the last intense terbium emission peak), thus confirming that the TG emission signal from AF594 must arise from FRET sensitization via TbL4.

Such antibodies with different possibilities of excitation and emission modes (different excitation and emission wavelengths, pulsed and CW excitation, and SS and TG detection) offer the possibility of tuning the imaging experiment toward reduced background emission (e.g., suppression of autofluorescence), reduced photobleaching (e.g., lower excitation power), and more efficient multiplexing (e.g., reduced spectral crosstalk).

QDs in FRET-Based Diagnostics. Although a successful transfer of QDs from research applications to commercial optical diagnostic assay kits has not been established, most probably because of the lack of stability, storability, and reproducibility of QD bioconjugates,[60] QDs are frequently used in a large variety of biological in vitro assays,[11,46−48,52,68,69,143−147] including detection of the enzyme activity and enzyme-based assays,[148−152] protein binding assays and FRET immunoassays,[47,153−157] DNA hybridization assays and aptamer-based assays,[59,103,158−163] as well as pH and ion sensing.[150,164−166] Because of their unique optical properties (mainly their size-tunable colors), QDs are often used for the multiplexed detection of several analytes within the same sample.[17,57−59,151,152,167]

In 2012, Freeman et al. developed aptamer-based optical sensors utilizing FRET for the quantitative detection of the vascular endothelial growth factor (VEGF), which was proposed as an important clinical biomarker for different diseases such as cancer (VEGF overexpression due to fast-growing tumor cells), Parkinson's disease (VEGF down-regulation due to neurological disorders), and Alzheimer's disease.[168] Aptamers are oligonucleotides with specific recognition properties toward proteins and can therefore be used in place of large antibodies in specific binding assays. The authors investigated different FRET-based detection strategies using anti-VEGF aptamers labeled to 620-nm-emitting CdSe/ZnS QDs as donors and black hole quenchers (BHQ) and Cy5 dyes as acceptors. Several chemiluminescence resonance energy-transfer-based sensing platforms were also tested but are not reviewed here. For the first FRET aptasensor, the anti-VEGF aptamer was labeled with QDs and a complementary DNA strand was labeled with BHQ in order to quench QD luminescence in the absence of VEGF due to hybridization of the quencher strand to the QD-labeled strand. The addition of VEGF led to separation of the duplex strands because of aptamer–VEGF binding, and thus FRET from QD to BHQ decreased while QD luminescence increased (Figure 8a). For the second FRET aptasensor, an anti-VEGF aptamer was split into two subunits, of which one was labeled with a QD donor and the other with a Cy5 acceptor. Upon VEGF addition, both subunits bound their target, which brought FRET donor and acceptor into close proximity and led to QD-to-Cy5 FRET. Because of energy transfer, QD luminescence was quenched and FRET-sensitized Cy5 emission appeared (Figure 8b). The third FRET aptasensor applied two aptamer subunits, of which one subunit was labeled with QDs and BHQs, respectively, as well as Exonuclease III (Exo III) as the analyte-recycling catalyst. In the absence of VEGF, QD luminescence was

dx.doi.org/10.1021/ic4017883 | Inorg. Chem. 2014, 53, 1824−1838

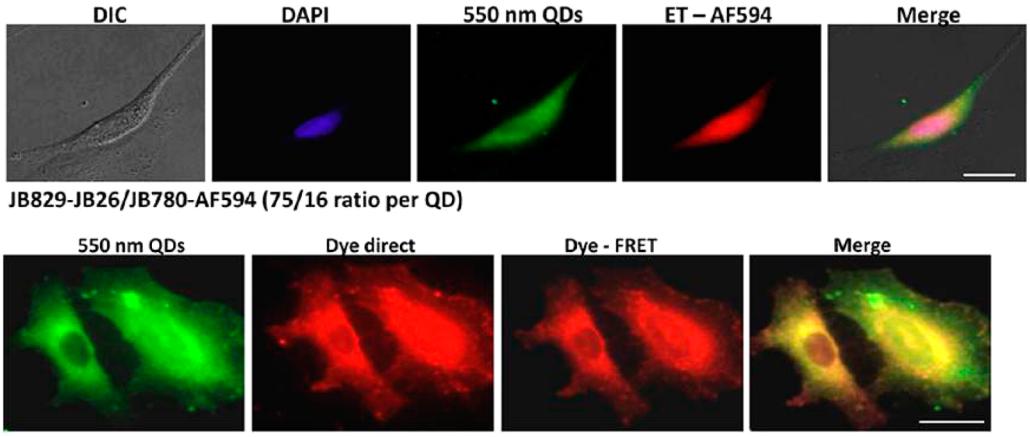

Figure 9. Fluorescence microscopy images obtained with different QD–peptide conjugates. Top: Images of A549 cells labeled with mixed QD–peptide conjugates bearing the CCP JB829-26 and the Alexa Fluor 594-labeled control peptide JB780–AF594 to investigate the cytosolic QD/AF594–peptide cargo delivery and stability (scale bar = 50 μM). The AF549 cells were incubated for 3 h with the QD/AF594–peptide conjugates and cultivated for 3 days prior to fixation. The QD550-to-AF594 FRET (panel ET-AF594) confirms the stability of the QD/AF594–peptide conjugates in cytosol after 3 days. Bottom: Images of the specific plasma membrane labeling of PC12-Adh cells. The cells were incubated sequentially with QD550–JB858 conjugates (1 h) and Rh-DHPE (20 min). Sensitized emission of Rh-DHPE acceptors due to FRET from the QD550 donors (panel Dye-FRET) shows colocalization at the cell membranes and thus the membrane-specific QD delivery by the JB585 peptide. Reproduced with permission from ref 177. Copyright 2013 American Chemical Society.

quenched via FRET to the BHQs. In the presence of VEGF, both aptamer subunits bind to the protein, and QD luminescence is still quenched. However, in this configuration, the coadded Exo III enzymes can digest the duplex (hybridized) aptamer strands from the 3′ end. The enzymatic digestion process releases BHQ and VEGF from the bound complex, which resulted in increasing QD luminescence and enabled the free VEGF to bind new (undigested) aptamer subunits (Figure 8c). This catalytic amplification enabled the lowering of the limit of detection (LOD) from 1 and 12 nM for the first and second aptasensors, respectively, and down to 5 pM for the Exo III-based aptasensor.

QDs in FRET-Based Imaging. Apart from their frequent use in FRET-based biosensing spectroscopy, QDs are also widely used for cellular imaging[46,48,146,169–175] and both QDs and QD–dye FRET pairs have been used together with different delivery techniques for target-specific imaging of various cellular compartments.[176] Because QDs are usually taken up by cells via endocytosis, the quick and efficient release of QDs from the endosomes to the cytosol is still a very important aspect of QD bioconjugates for cellular imaging. In this direction, Boeneman et al. recently demonstrated the cytosolic delivery of different proteins, nanoparticles (including QDs), and dendrimers to various cell types using improved CCPs.[177] The authors used derivatives of the peptide JB577 (originally designed to deliver palmitoyl–protein thioesterase inhibitors to neurons), which has the ability to mediate cytosolic delivery of QDs to a wide range of cell types in a nontoxic manner, and to facilitate the efficient endosomal escape of small and large proteins, dendrimers, and other nanomaterials such as AuNPs. First, the activity relationship of the modular JB peptide was investigated by modifying its length, charge, fatty acid content, and sequence order to identify the key motifs and best sequence for efficient endosomal escape. Various peptide candidates were then tested concerning their QD delivery mediation (peptide/QD labeling ratio, incubation time, etc.), their applicability for different cell types (PC12, HeLa, and HEK cells, as well as primary dermal fibroplasts), and their cytosolic delivery mediation for disparate proteins and nanomaterials (QDs, maltose binding proteins, β-phycoerythrin, G5-PAMAM dendrimers, and 8.2 nm AuNPs). In a next step, different JB577 variants were used to quantify the QD uptake. Thereby, a sequence modified by one methylene group (JB858) was discovered, which specifically targets QDs to cellular membranes. Finally, cellular labeling was performed using multiple cargos (different-colored peptide–QD conjugates and fluorescent dye-labeled peptides) with different peptide variants. To verif, that the QD–peptide conjugates enabled the cytosolic delivery of an additional cargo, FRET from 550-nm-emitting QD (QD550) donors to Alexa Fluor 594 (AF594) acceptors was utilized. QD550 conjugates labeled with the CCP JB829-26 and the AF594-labeled control peptide (JB780–AF594) were delivered to A549 cells. FRET microscopy revealed that the mixed QD-donor/AF594-acceptor peptide conjugates remained intact within the cytosol over 3 days (Figure 9, top), demonstrating their possible use as intracellular FRET-based sensors without the need for toxic transfection reagents and invasive microinjection. Furthermore, QD550–JB585 conjugates were used to label the plasma membranes of PC12-Adh cells. The membrane selectivity was demonstrated by FRET from the QD550 donors to Lissamine rhodamine B derivatives (Rh-DHPE) as FRET acceptors. Rh-DHPE is an amphiphilic dye containing two hexadecanoic ester groups and is routinely used to stain cell membranes. Hence, FRET from QD550 to Rh-DHPE confirms colocalization of the QD–JB585 peptide conjugates and amphiphilic Rh-DHPE at the plasma membranes (Figure 9, bottom).

Combination of LLLs and QDs in FRET. As was already mentioned in the FRET section, the application of LLLs and QDs as a donor–acceptor pair offers several advantages for optical biosensing. This unique FRET pair can provide high sensitivity, multiplexing capability, and measurement over relatively large FRET distances. Because the use of QDs as acceptors was predicted to be a very challenging task and shown to be impossible or at least extremely inefficient using conventional organic dye fluorophores,[178] our initial studies focused on the demonstration of FRET from LLLs to QDs using the frequently applied streptavidin–biotin binding. In

dx.doi.org/10.1021/ic4017883 | Inorg. Chem. 2014, 53, 1824–1838

fact, we could show that europium and terbium complexes labeled to streptavidin can efficiently sensitize biotinylated QDs in close proximity to the LLLs because of the streptavidin−biotin recognition.[95,96,98] Taking advantage of the color tunability of QD, we extended these proof-of-principles to multiplexed detection using up to five different QDs, which were all excited by the same type of terbium complex. Such 5-fold multiplexed assays showed very high sensitivity (up to ca. 250-fold lower detection limits compared to the Eu-TBP−APC FRET pair applied in commercial HTRF assays) and the possibility of being used as a multiplexed molecular ruler for determination of the QD sizes and shapes under physiological conditions at subnanomolar concentrations.[17,179,180] In order to use the LLL-to-QD FRET for biomarker detection, our and other groups have applied this technology to immunoassays for detection of estradiol in a competitive assay[97] and α-fetoprotein,[99] prostate-specific antigen,[181] and epidermal growth factor receptor[182] in noncompetitive sandwich assays. In a recent study (new and so-far-unpublished data), we developed such a sandwich immunoassay using commercially available LLLs and QDs, namely, TbL4 and Qdot655 (Invitrogen and Life Technologies), to detect the tumor marker CEA. The assay was performed on a KRYPTOR immunoreader using the same antibody clones (but conjugated with TbL4 and Qdot655) as used within the commercial KRYPTOR CEA assay kits. The assay consisted of 40 μL of each antibody conjugate, to which 70 μL serum samples with increasing CEA concentrations were added. The immunoassay calibration curve (showing the TG intensity ratio of QD and terbium emission over the CEA concentration within the 70 μL samples) is displayed in Figure 10. The LOD was calculated using slope m of the linearly increasing part of the calibration curve (inset of Figure 10, $m = 1.76 \times 10^{-4}$ $(\text{ng/mL})^{-1}$) and the standard deviation σ of the measured intensity ratio at zero CEA concentration $[\sigma(0) = 1.52 \times 10^{-4}]$, applying the equation LOD = $3\sigma(0)/m$ = 2.6 ng/mL. This LOD is below the clinical cutoff value of 5 ng/mL CEA in the serum of a healthy person, which means that the Tb-to-QD FRET assay is sensitive enough to be used in clinical diagnostics of CEA.

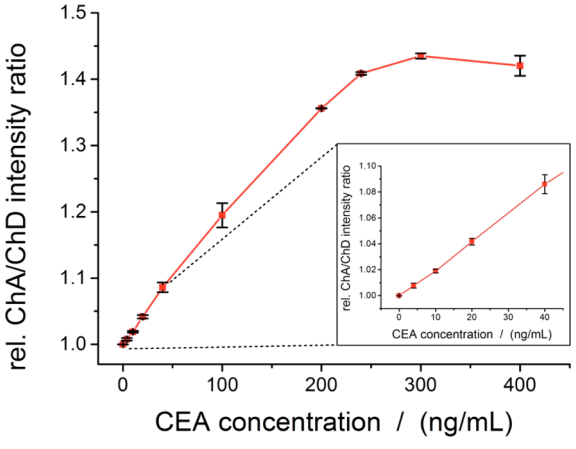

Figure 10. Calibration curve of the homogeneous Tb-to-QD FRET immunoassays for CEA. Displayed are the relative ratios of the TG luminescence intensities measured in the QD acceptor channel (660 ± 6 nm) and in the terbium donor channel (620 ± 5 nm) with the KRYPTOR immunoreader in a time window of 50−450 μs after pulsed UV excitation as a function of the CEA concentration. The inset shows the linear range of the obtained calibration curve that was used to calculate the LOD for CEA in this FRET immunoassay. *Note: This is new and so-far-unpublished data.*

Because QDs have a relatively large surface, they can be used as scaffolds for attaching many biomolecular recognition molecules against the same or different targets. Apart from antibodies, proteins, or biotin, we have also used peptides and oligonucleotides, which were self-assembled to the QD surfaces via polyhistidine, to establish Tb-to-QD FRET-based biosensors.[151,183,184] We took advantage of these multilabeled QDs to establish so-called FRET relays, for which two independent FRET steps can be performed with a single QD functioning as a simultaneous donor and acceptor, as illustrated in Scheme 1.

Scheme 1. FRET Relays: Terbium Complexes and Dyes (Both Conjugated with Peptides or Oligonucleotides) are Coassembled on the Same QD[a]

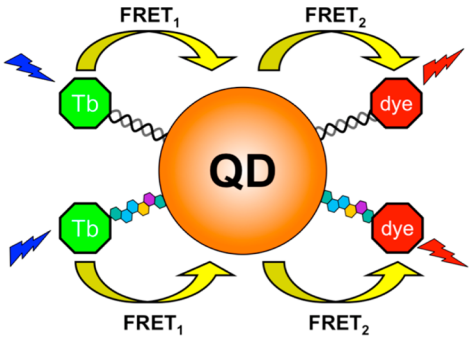

[a]Pulsed excitation in UV leads to excited terbium and QD and prompt FRET from QD to dye ($FRET_2$). After a delay of several microseconds, there is still much terbium in the excited state, whereas the QD has decayed to its ground state, and efficient time-delayed FRET from terbium to QD ($FRET_1$) becomes possible. The newly excited QD can then sensitize again the dyes by TG $FRET_2$.

Pulsed excitation in UV leads to prompt FRET from QD to dye ($FRET_2$) and TG FRET (after a delay of several microseconds) from terbium to QD to dye ($FRET_1$ + $FRET_2$). The independence of these two FRET processes could be used for spectrotemporal multiplexing, which allowed measurement of the duplexed DNA hybridization assays and duplexed enzyme kinetics using only one QD color.[151,184] Such multistep FRET assemblies demonstrate the large flexibility of using QDs in combination with different FRET donors and acceptors, which will also offer many benefits for highly sensitive multiplexed cellular biosensing.

SUMMARY AND OUTLOOK

LLLs and QDs are very unique fluorophores with large advantages concerning high sensitivity and multiplexing within FRET-based biosensing. LLL-FRET-based diagnostics has already advanced far beyond basic research and is broadly used in commercial assay kits for clinical diagnostics applied in clinical studies as well as clinical laboratories or emergency room testing. LLL-based FRET imaging is a much younger and less advanced field mainly because of the less common TG imaging equipment. Nevertheless, this field offers large opportunities because reduced autofluorescence background by time gating of the long-lived LLL luminescence can be especially advantageous for cell and tissue imaging. The application of QD-based FRET has increased tremendously over the last 2 decades, which has mainly been caused by the

dx.doi.org/10.1021/ic4017883 | Inorg. Chem. 2014, 53, 1824−1838

benefits related to the nanoparticle structure and color tunability. Both spectroscopy and microscopy for diagnostics and cellular imaging are research fields in which QDs are often applied for high sensitivity and multiplexed detection. Problems that need to be solved for QD biosensing are the long-term stability and reproducibility of QD bioconjugates for commercial QD-based assay kits and efficient and fast cellular delivery. Being already quite advanced in research, it can be expected that the industry will pick up these topics and further optimize QD bioconjugates in order to integrate the advantages of QDs into commercial biosensing applications such as clinical diagnostics. The most promising trend for the future will be the exploitation of flexible FRET combinations, as we have already demonstrated by multistep FRET from LLLs to QDs to dyes for spectrotemporal multiplexing. By taking advantage of the large nanoparticle surfaces, the flexibility of biomolecules and bioconjugation, and the broad photophysical (e.g., spectral and temporal) versatility of the available fluorophores, FRET will still offer many opportunities for future biosensing applications.

MATERIALS AND METHODS FOR THE NEW DATA PRESENTED IN THIS ARTICLE

Cellular Imaging Using TbL4−AF594 Antibodies. Optically trifunctional antibodies were prepared by mixing Alexa Fluor 594 goat antirabbit IgG (Life Technologies) with an excess of Lumi4-Tb-NHS in 100 mM carbonate buffer (pH 9.0) and incubating for 2 h at room temperature. BJ-hTERT cells were kindly provided by Prof. O. Söderberg (Uppsala University, Uppsala, Sweden). Cells were cultured at 37 °C and 5% CO_2 in Dulbecco's modified eagle medium supplemented with 2 mM L-glutamine, 10% fetal bovine serum, and antibiotics antimycotic (Gibco). Cells were incubated overnight before immune-fluorescent staining. For staining, cells were fixed with 4% paraformaldehyde in phosphate buffered saline (PBS) and blocked for 1 h with PBS containing 1% bovine serum albumin (BSA). The samples were then incubated with a primary antibody, antirabbit PDGFR-β (cell signaling), for 3 h followed by a washing step and 1 h of incubation with secondary antibodies, AF594 goat antirabbit or TbL4−AF594 goat antirabbit IgG. After washing, the samples were mounted using a Prolong Gold Antifade mounting medium (Life Technologies) and imaged. The samples were imaged using an inverted microscope (Olympus IX71) equipped with a CW excitation source (X-Cite 120Q) and a camera (Scientific CMOS pco.edge) for SS detection. For TG images, a pulsed laser emitting at 349 nm (Spectra Physics) in combination with an ICCD camera (PI-MAX 3, Princeton Instruments) was used. All images were acquired with a 40× objective. Band-pass filters for the different channels are specified in the figures. For TG imaging, conditions were 100 Hz laser repetition rate, 40 ICCD gain, 10 μs detection delay, 2 ms detection gate width, and 500 gates/exposure. Excitation/emission spectra and luminescence decay curves were obtained on a FluoTime 300 fluorescence lifetime spectrometer (PicoQuant) from antibody samples diluted in PBS.

Tb-to-QD FRET Immunoassays for CEA. Assay was performed on a modified KRYPTOR immunoreader with two PMT detection channels for ratiometric acceptor/donor TG intensity measurements. Separation of donor and acceptor emission was achieved by using a dichroic mirror (Delta) with a sharp transmission cutoff between 630 and 640 nm and band-pass filters for the terbium donor channel (620 ± 5 nm, KRYPTOR) and the QD acceptor channel (660 ± 6 nm, Semrock). A 337.1 nm nitrogen laser with a 20 Hz repetition rate and ca. 60 μJ pulse energy was used as the excitation source. Antibody conjugates were ca. 1.3 nM Lumi4Tb-labeled GFR44 anti-CEA donor antibodies (labeling ratio of 4.4 for Lumi4Tb/GFR44) and ca. 5 nM QDot655-labeled G15 anti-CEA acceptor antibodies (labeling ratio of approximately 3 for G15/QDot655) in 100 mM Tris buffer (pH 7) containing 0.1% BSA. A total of 40 μL of each antibody conjugate solution was mixed in KRYPTOR multiwell plates with 70 μL of antigen sample containing different CEA concentrations ranging from 0 to 400 ng/mL. After 90 min of incubation at room temperature, each well was measured with 800 flashes (40 s/well) and the TG luminescence intensities were detected in the donor and acceptor detection channels within a time window from 50 to 450 μs after excitation pulses. The intensity ratios (acceptor/donor) were used for the calibration curves.

ASSOCIATED CONTENT

Supporting Information

FRET literature statistics (Figure S1), FRET areas of research (Table S1), FRET distance dependence (Figure S2), and Tb-based cellular imaging (Figure S3). This material is available free of charge via the Internet at http://pubs.acs.org.

AUTHOR INFORMATION

Corresponding Author

*E-mail: niko.hildebrandt@u-psud.fr.

Notes

The authors declare no competing financial interest.

ACKNOWLEDGMENTS

We thank Lumiphore, Inc., for the gift of the Lumi4-Tb-NHS reagent and the European Commission (FP7 Project NANOGNOSTICS), the European Innovative Medicines Initiative IMI (Project OncoTrack), the Investissements d'Avenir Program France (Project NanoCTC), and the Agence National de la Recherche France (Project NanoFRET) for financial support.

REFERENCES

(1) Clegg, R. M. In *Reviews in Fluorescence*; Geddes, C., Lakowicz, J., Eds.; Springer: New York, 2006; Vol. *2006*, p 1.
(2) Förster, T. *Naturwissenschaften* **1946**, *33*, 166.
(3) Förster, T. *Ann. Phys.* **1948**, *437*, 55.
(4) Förster, T. *Discuss. Faraday Soc.* **1959**, *27*, 7.
(5) Stryer, L.; Haugland, R. P. *Proc. Natl. Acad. Sci. U.S.A.* **1967**, *58*, 719.
(6) Clegg, R. M. In *Fluorescence Imaging Spectroscopy and Microscopy*; Wang, X. F., Herman, B., Eds.; John Wiley and Sons, Inc.: New York, 1996; Vol. *137*, p 179.
(7) Szöllosi, J.; Damjanovich, S.; Mátyus, L. *Cytometry* **1998**, *34*, 159.
(8) Selvin, P. R. *Nat. Struct. Biol.* **2000**, *7*, 730.
(9) Jares-Erijman, E. A.; Jovin, T. M. *Nat. Biotechnol.* **2003**, *21*, 1387.
(10) Lakowicz, J. R. *Principles of Fluorescence Spectroscopy*, 3rd ed.; Springer: Berlin, 2006.
(11) Sapsford, K. E.; Berti, L.; Medintz, I. L. *Angew. Chem., Int. Ed.* **2006**, *45*, 4562.
(12) Braslavsky, S. E.; Fron, E.; Rodriguez, H. B.; Roman, E. S.; Scholes, G. D.; Schweitzer, G.; Valeur, B.; Wirz, J. *Photochem. Photobiol. Sci.* **2008**, *7*, 1444.
(13) Clegg, R. M. In *Laboratory Techniques in Biochemistry and Molecular*; Gadella, T. W. J., Ed.; Elsevier BV: Amsterdam, The Netherlands, 2009; Vol. *33*.
(14) Geißler, D.; Hildebrandt, N. *Curr. Inorg. Chem.* **2011**, *1*, 17.
(15) Sahoo, H. *J. Photochem. Photobiol., C* **2011**, *12*, 20.
(16) Medintz, I. L.; Hildebrandt, N. *FRET—Förster Resonance Energy Transfer. From Theory to Applications*; Wiley-VCH: Weinheim, Germany, 2013.
(17) Geißler, D.; Charbonniere, L. J.; Ziessel, R. F.; Butlin, N. G.; Löhmannsröben, H.-G.; Hildebrandt, N. *Angew. Chem., Int. Ed.* **2010**, *49*, 1396.
(18) Charbonnière, L. J.; Hildebrandt, N. *Eur. J. Inorg. Chem.* **2008**, *2008*, 3241.
(19) Hemmilä, I.; Ståhlberg, T.; Mottram, P. *Wallac Bioanalytical Applications of Labelling Technologies: A Review of Trends and*

Opportunities in Biospecific Assay Based on the Product Offering of Wallac; Wallac Oy, an EG & G Co.; Turku, Finland, 1994.
(20) Charbonniere, L.; Ziessel, R.; Guardigli, M.; Roda, A.; Sabbatini, N.; Cesario, M. *J. Am. Chem. Soc.* **2001**, *123*, 2436.
(21) Bünzli, J.-C. G.; Piguet, C. *Chem. Soc. Rev.* **2005**, *34*, 1048.
(22) Pandya, S.; Yu, J. H.; Parker, D. *Dalton Trans.* **2006**, 2757.
(23) Brunet, E.; Juanes, O.; Rodriguez-Ubis, J. C. *Curr. Chem. Biol.* **2007**, *1*, 11.
(24) de Bettencourt-Dias, A. *Curr. Org. Chem.* **2007**, *11*, 1460.
(25) Bünzli, J. C. G. *Chem. Rev.* **2010**, *110*, 2729.
(26) Eliseeva, S. V.; Bunzli, J. C. G. *Chem. Soc. Rev.* **2010**, *39*, 189.
(27) Butler, S. J.; Parker, D. *Chem. Soc. Rev.* **2013**, *42*, 1652.
(28) Hovinen, J.; Guy, P. M. *Bioconjugate Chem.* **2009**, *20*, 404.
(29) Charbonnière, L. J. *Curr. Inorg. Chem.* **2011**, *1*, 2.
(30) Alpha, B.; Lehn, J. M.; Mathis, G. *Angew. Chem., Int. Ed. Engl.* **1987**, *26*, 266.
(31) Alpha, B.; Ballardini, R.; Balzani, V.; Lehn, J. M.; Perathoner, S.; Sabbatini, N. *Photochem. Photobiol.* **1990**, *52*, 299.
(32) Brunet, E.; Juanes, O.; Sedano, R.; Rodriguez-Ubis, J. C. *Photochem. Photobiol. Sci.* **2002**, *1*, 613.
(33) Petoud, S.; Cohen, S. M.; Bunzli, J. C. G.; Raymond, K. N. *J. Am. Chem. Soc.* **2003**, *125*, 13324.
(34) Weibel, N.; Charbonnière, L. J.; Guardigli, M.; Roda, A.; Ziessel, R. F. *J. Am. Chem. Soc.* **2004**, *126*, 4888.
(35) Starck, M.; Kadjane, P.; Bois, E.; Darbouret, B.; Incamps, A.; Ziessel, R.; Charbonniere, L. J. *Chem.—Eur. J.* **2011**, *17*, 9164.
(36) Xu, J.; Corneillie, T. M.; Moore, E. G.; Law, G.-L.; Butlin, N. G.; Raymond, K. N. *J. Am. Chem. Soc.* **2011**, *133*, 19900.
(37) Walton, J. W.; Bourdolle, A.; Butler, S. J.; Soulie, M.; Delbianco, M.; McMahon, B. K.; Pal, R.; Puschmann, H.; Zwier, J. M.; Lamarque, L.; Maury, O.; Andraud, C.; Parker, D. *Chem. Commun.* **2013**, *49*, 1600.
(38) D'Aleo, A.; Picot, A.; Beeby, A.; Williams, J. A. G.; Le Guennic, B.; Andraud, C.; Maury, O. *Inorg. Chem.* **2008**, *47*, 10258.
(39) Kong, H. K.; Chadbourne, F. L.; Law, G. L.; Li, H. G.; Tam, H. L.; Cobb, S. L.; Lau, C. K.; Lee, C. S.; Wong, K. L. *Chem. Commun.* **2011**, *47*, 8052.
(40) Lamarque, M.; Maury, O.; Parker, D.; Zwier, J.; Walton, J. W.; Bourdolle, A. French PatentWO2013/011236A1, 2012.
(41) Alivisatos, A. P. *Science* **1996**, *271*, 933.
(42) Efros, A. L.; Rosen, M. *Annu. Rev. Mater. Sci.* **2000**, *30*, 475.
(43) Murphy, C. J.; Coffer, J. L. *Appl. Spectrosc.* **2002**, *56*, 16A.
(44) Dabbousi, B. O.; Rodriguez-Viejo, J.; Mikulec, F. V.; Heine, J. R.; Mattoussi, H.; Ober, R.; Jensen, K. F.; Bawendi, M. G. *J. Phys. Chem. B* **1997**, *101*, 9463.
(45) Reiss, P.; Protiere, M.; Li, L. *Small* **2009**, *5*, 154.
(46) Petryayeva, E.; Algar, W. R.; Medintz, I. L. *Appl. Spectrosc.* **2013**, *67*, 215.
(47) Esteve-Turrillas, F. A.; Abad-Fuentes, A. *Biosens. Bioelectron.* **2013**, *41*, 12.
(48) Medintz, I. L.; Uyeda, H. T.; Goldman, E. R.; Mattoussi, H. *Nat. Mater.* **2005**, *4*, 435.
(49) Algar, W. R.; Tavares, A. J.; Krull, U. J. *Anal. Chim. Acta* **2010**, *673*, 1.
(50) Zhang, Y.; Clapp, A. R. *Sensors* **2011**, *11*, 11036.
(51) Sperling, R. A.; Parak, W. J. *Philos. Trans. R. Soc. A* **2010**, *368*, 1333.
(52) Algar, W. R.; Susumu, K.; Delehanty, J. B.; Medintz, I. L. *Anal. Chem.* **2011**, *83*, 8826.
(53) Horoz, S.; Lu, L. Y.; Dai, Q. L.; Chen, J. J.; Yakami, B.; Pikal, J. M.; Wang, W. Y.; Tang, J. K. *Appl. Phys. Lett.* **2012**, *101*, 223902.
(54) Wang, Q. S.; Fang, T. T.; Liu, P.; Deng, B. H.; Min, X. M.; Li, X. *Inorg. Chem.* **2012**, *51*, 9208.
(55) Jennings, T. L.; Becker-Catania, S. G.; Triulzi, R. C.; Tao, G. L.; Scott, B.; Sapsford, K. E.; Spindel, S.; Oh, E.; Jain, V.; Delehanty, J. B.; Prasuhn, D. E.; Boeneman, K.; Algar, W. R.; Medintz, I. L. *ACS Nano* **2011**, *5*, 5579.
(56) Sapsford, K. E.; Algar, W. R.; Berti, L.; Gemmill, K. B.; Casey, B. J.; Oh, E.; Stewart, M. H.; Medintz, I. L. *Chem. Rev.* **2013**, *113*, 1904.
(57) Chan, W. C. W.; Maxwell, D. J.; Gao, X.; Bailey, R. E.; Han, M.; Nie, S. *Curr. Opin. Biotechnol.* **2002**, *13*, 40.
(58) Clapp, A. R.; Medintz, I. L.; Uyeda, H. T.; Fisher, B. R.; Goldman, E. R.; Bawendi, M. G.; Mattoussi, H. *J. Am. Chem. Soc.* **2005**, *127*, 18212.
(59) Algar, W. R.; Krull, U. J. *Anal. Chem.* **2009**, *81*, 4113.
(60) Hildebrandt, N. *ACS Nano* **2011**, *5*, 5286.
(61) Resch-Genger, U.; Grabolle, M.; Cavaliere-Jaricot, S.; Nitschke, R.; Nann, T. *Nat. Methods* **2008**, *5*, 763.
(62) Li, J.; Zhang, J. Z. *Coord. Chem. Rev.* **2009**, *253*, 3015.
(63) Sanderson, K. *Nature* **2009**, *459*, 760.
(64) Ruhle, S.; Shalom, M.; Zaban, A. *ChemPhysChem* **2010**, *11*, 2290.
(65) Buhbut, S.; Itzhakov, S.; Oron, D.; Zaban, A. *J. Phys. Chem. Lett.* **2011**, *2*, 1917.
(66) Bruchez, M.; Moronne, M.; Gin, P.; Weiss, S.; Alivisatos, A. P. *Science* **1998**, *281*, 2013.
(67) Chan, W. C. W.; Nie, S. *Science* **1998**, *281*, 2016.
(68) Frasco, M. F.; Chaniotakis, N. *Anal. Bioanal. Chem.* **2010**, *396*, 229.
(69) Medintz, I. L.; Mattoussi, H. *Phys. Chem. Chem. Phys.* **2009**, *11*, 17.
(70) Derfus, A. M.; Chan, W. C. W.; Bhatia, S. N. *Nano Lett.* **2004**, *4*, 11.
(71) Hardman, R. *Environ. Health Perspect.* **2006**, *114*, 165.
(72) Bradburne, C. E.; Delehanty, J. B.; Boeneman-Gemmill, K.; Mei, B. C.; Susumu, K.; Blanco-Canosa, J. B.; Dawson, P. E.; Mattoussi, H.; Medintz, I. L. *Bioconjugate Chem.* **2013**, DOI: 10.1021/bc4001917.
(73) Van Der Meer, B. W.; Coker, G.; Chen, S.-Y. S. *Resonance Energy Transfer: Theory and Data*; Wiley-VCH: Weinheim, Germany, 1994.
(74) Valeur, B. *Molecular Fluorescence: Principles and Applications*; Wiley-VCH: Weinheim, Germany, 2002.
(75) Van der Meer, B. W. *Rev. Mol. Biotechnol.* **2002**, *82*, 181.
(76) Van der Meer, B. W. In *FRET—Förster Resonance Energy Transfer. From Theory to Applications*; Medintz, I. L., Hildebrandt, N., Eds.; Wiley-VCH: Weinheim, Germany, 2013.
(77) Horrocks, W. D.; Rhee, M. J.; Snyder, A. P.; Sudnick, D. R. *J. Am. Chem. Soc.* **1980**, *102*, 3650.
(78) Joshi, N. B.; Shamoo, A. E. *Eur. J. Biochem.* **1988**, *178*, 483.
(79) Selvin, P. R. *IEEE J. Sel. Top. Quantum Electron.* **1996**, *2*, 1077.
(80) Richardson, F. S. *Chem. Rev.* **1982**, *82*, 541.
(81) Bünzli, J.-C. G. *Lanthanide Probes in Life, Chemical and Earth Science: Theory and Practice*; Elsevier: Amsterdam, The Netherlands, 1989.
(82) Laitala, V.; Hemmila, L. *Anal. Chem.* **2005**, *77*, 1483.
(83) Vuojola, J.; Lamminmaki, U.; Soukka, T. *Anal. Chem.* **2009**, *81*, 5033.
(84) Haugland, R. P. *The Molecular Probes® Handbook—A Guide to Fluorescent Probes and Labeling Technologies*, 11th ed.; Life Technologies Corp.: Carlsbad, CA, 2010.
(85) Hötzer, B.; Medintz, I. L.; Hildebrandt, N. *Small* **2012**, *8*, 2297.
(86) Sapsford, K. E.; Wildt, B.; Mariani, A.; Yeatts, A. B.; Medintz, I. L. In *FRET—Förster Resonance Energy Transfer. From Theory to Applications*; Medintz, I. L., Hildebrandt, N., Eds.; Wiley-VCH: Weinheim, Germany, 2013.
(87) Mathis, G. *Clin. Chem.* **1993**, *39*, 1953.
(88) Byrne, A. G.; Byrne, M. M.; Coker, G.; Boeneman-Gemmill, K.; Spillmann, C.; Medintz, I. L.; Sloan, S. L.; Van der Meer, B. W. In *FRET—Förster Resonance Energy Transfer. From Theory to Applications*; Medintz, I. L., Hildebrandt, N., Eds.; Wiley-VCH: Weinheim, Germany, 2013.
(89) Freeman, R.; Willner, I. *Chem. Soc. Rev.* **2012**, *41*, 4067.
(90) Algar, W. R.; Massey, M.; Krull, U. J. In *FRET—Förster Resonance Energy Transfer. From Theory to Applications*; Medintz, I. L., Hildebrandt, N., Eds.; Wiley-VCH: Weinheim, Germany, 2013.
(91) Algar, W. R.; Kim, H.; Medintz, I. L.; Hildebrandt, N. *Coord. Chem. Rev.* **2013**, DOI: 10.1016/j.ccr.2013.07.015.

(92) Rogach, A. L.; Klar, T. A.; Lupton, J. M.; Meijerinkd, A.; Feldmann, J. *J. Mater. Chem.* **2009**, *19*, 1208.
(93) Roberti, M. J.; Giordano, L.; Jovin, T. M.; Jares-Erijman, E. A. *ChemPhysChem* **2011**, *12*, 563.
(94) Bednarkiewicz, A.; Nyk, M.; Samoc, M.; Strek, W. *J. Phys. Chem. C* **2010**, *114*, 17535.
(95) Hildebrandt, N.; Charbonniere, L. J.; Beck, M.; Ziessel, R. F.; Löhmannsröben, H.-G. *Angew. Chem., Int. Ed.* **2005**, *44*, 7612.
(96) Charbonnière, L. J.; Hildebrandt, N.; Ziessel, R. F.; Löhmannsröben, H.-G. *J. Am. Chem. Soc.* **2006**, *128*, 12800.
(97) Härmä, H.; Soukka, T.; Shavel, A.; Gaponik, N.; Weller, H. *Anal. Chim. Acta* **2007**, *604*, 177.
(98) Hildebrandt, N.; Charbonnière, L. J.; Löhmannsröben, H.-G. *J. Biomed. Biotechnol.* **2007**, 79169.
(99) Chen, M. J.; Wu, Y. S.; Lin, G. F.; Hou, J. Y.; Li, M.; Liu, T. C. *Anal. Chim. Acta* **2012**, *741*, 100.
(100) So, M. K.; Xu, C. J.; Loening, A. M.; Gambhir, S. S.; Rao, J. H. *Nat. Biotechnol.* **2006**, *24*, 339.
(101) Yao, H.; Zhang, Y.; Xiao, F.; Xia, Z.; Rao, J. *Angew. Chem., Int. Ed.* **2007**, *46*, 4346.
(102) Zhao, S. L.; Huang, Y.; Liu, R. J.; Shi, M.; Liu, Y. M. *Chem.—Eur. J.* **2010**, *16*, 6142.
(103) Freeman, R.; Liu, X. Q.; Willner, I. *J. Am. Chem. Soc.* **2011**, *133*, 11597.
(104) Selvin, P. R. *Annu. Rev. Biophys. Biomol. Struct.* **2002**, *31*, 275.
(105) Hagan, A. K.; Zuchner, T. *Anal. Bioanal. Chem.* **2011**, *400*, 2847.
(106) Liu, Y. S.; Tu, D. T.; Zhu, H. M.; Ma, E.; Chen, X. Y. *Nanoscale* **2013**, *5*, 1369.
(107) Soukka, T.; Kuningas, K.; Rantanen, T.; Haaslahti, V.; Lövgren, T. *J. Fluoresc.* **2005**, *15*, 513.
(108) Guo, H. C.; Sun, S. Q. *Nanoscale* **2012**, *4*, 6692.
(109) Soini, E.; Hemmila, I. *Clin. Chem.* **1979**, *25*, 353.
(110) Morrison, L. E. *Anal. Biochem.* **1988**, *174*, 101.
(111) Dickson, E. F. G.; Pollak, A.; Diamandis, E. P. *J. Photochem. Photobiol., B* **1995**, *27*, 3.
(112) Hemmilä, I.; Mukkala, V. M.; Takalo, H. *J. Alloys Compd.* **1997**, *249*, 158.
(113) Hemmilä, I.; Laitala, V. *J. Fluoresc.* **2005**, *15*, 529.
(114) Riddle, S. M.; Vedvik, K. L.; Hanson, G. T.; Vogel, K. W. *Anal. Biochem.* **2006**, *356*, 108.
(115) Härmä, H.; Sarrail, G.; Kirjavainen, J.; Martikkala, E.; Hemmilä, I.; Hänninen, P. *Anal. Chem.* **2010**, *82*, 892.
(116) Stryer, L. *Annu. Rev. Biochem.* **1978**, *47*, 819.
(117) Xiao, M.; Li, H.; Snyder, G. E.; Cooke, R.; Yount, R. G.; Selvin, P. R. *Proc. Natl. Acad. Sci. U.S.A.* **1998**, *95*, 15309.
(118) Appelblom, H.; Nurmi, J.; Soukka, T.; Pasternack, M.; Penttila, K. E.; Lövgren, T.; Niemela, P. *J. Biomol. Screening* **2007**, *12*, 842.
(119) Tsourkas, A.; Behlke, M. A.; Xu, Y. Q.; Bao, G. *Anal. Chem.* **2003**, *75*, 3697.
(120) Santangelo, P. J.; Nix, B.; Tsourkas, A.; Bao, G. *Nucleic Acids Res.* **2004**, *32*, e57.
(121) Krasnoperov, L. N.; Marras, S. A. E.; Kozlov, M.; Wirpsza, L.; Mustaev, A. *Bioconjugate Chem.* **2010**, *21*, 319.
(122) Mathis, G. *J. Biomol. Screening* **1999**, *4*, 309.
(123) Hemmilä, I. *J. Biomol. Screening* **1999**, *4*, 303.
(124) Reddy, D. R.; Rosa, L. E. P.; Miller, L. W. *Bioconjugate Chem.* **2011**, *22*, 1402.
(125) Yapici, E.; Reddy, D. R.; Miller, L. W. *ChemBioChem* **2012**, *13*, 553.
(126) Kim, B.; Tarchevskaya, S. S.; Eggel, A.; Vogel, M.; Jardetzky, T. S. *Anal. Biochem.* **2012**, *431*, 84.
(127) Kupcho, K. R.; Stafslien, D. K.; DeRosier, T.; Hallis, T. M.; Ozers, M. S.; Vogel, K. W. *J. Am. Chem. Soc.* **2007**, *129*, 13372.
(128) Kokko, T.; Kokko, L.; Soukka, T. *J. Fluoresc.* **2009**, *19*, 159.
(129) Kim, S. H.; Gunther, J. R.; Katzenellenbogen, J. A. *J. Am. Chem. Soc.* **2010**, *132*, 4685.
(130) Geißler, D.; Stufler, S.; Löhmannsröben, H.-G.; Hildebrandt, N. *J. Am. Chem. Soc.* **2013**, *135*, 1102.
(131) Di, W.; Li, J.; Shirahata, N.; Sakka, Y. *Nanotechnology* **2010**, *21*, 455703.
(132) Gu, J. Q.; Shen, J.; Sun, L. D.; Yan, C. H. *J. Phys. Chem. C* **2008**, *112*, 6589.
(133) Liu, Y. S.; Zhou, S. Y.; Tu, D. T.; Chen, Z.; Huang, M. D.; Zhu, H. M.; Ma, E.; Chen, X. Y. *J. Am. Chem. Soc.* **2012**, *134*, 15083.
(134) Rantanen, T.; Jarvenpaa, M.-L.; Vuojola, J.; Arppe, R.; Kuningas, K.; Soukka, T. *Analyst* **2009**, *134*, 1713.
(135) Chen, R.; Ta, V. D.; Xiao, F.; Zhang, Q. Y.; Sun, H. D. *Small* **2013**, *9*, 1052.
(136) Shomali, W.; Hachem, R.; Chaftari, A. M.; Jiang, Y.; Bahu, R.; Jabbour, J.; Raad, S.; Al Shuaibi, M.; Al Wohoush, I.; Raad, I. *Cancer—Am Cancer Soc.* **2012**, *118*, 5823.
(137) Seveus, L.; Vaisala, M.; Syrjanen, S.; Sandberg, M.; Kuusisto, A.; Harju, R.; Salo, J.; Hemmilä, I.; Kojola, H.; Soini, E. *Cytometry* **1992**, *13*, 329.
(138) Vereb, G.; Jares-Erijman, E.; Selvin, P. R.; Jovin, T. M. **1998**, *74*, 2210.
(139) Hanaoka, K.; Kikuchi, K.; Kobayashi, S.; Nagano, T. *J. Am. Chem. Soc.* **2007**, *129*, 13502.
(140) Rajapakse, H. E.; Reddy, D. R.; Mohandessi, S.; Butlin, N. G.; Miller, L. W. *Angew. Chem., Int. Ed.* **2009**, *48*, 4990.
(141) Rajapakse, H. E.; Miller, L. W. *Method Enzymol.* **2012**, *505*, 329.
(142) Mohandessi, S.; Rajendran, M.; Magda, D.; Miller, L. W. *Chem.—Eur. J.* **2012**, *18*, 10825.
(143) Alivisatos, A. P. *Nat. Biotechnol.* **2004**, *22*, 47.
(144) Gill, R.; Zayats, M.; Willner, I. *Angew. Chem., Int. Ed.* **2008**, *47*, 7602.
(145) Algar, W. R.; Krull, U. J. *Anal. Bioanal. Chem.* **2010**, *398*, 2439.
(146) Jin, Z. W.; Hildebrandt, N. *Trends Biotechnol.* **2012**, *30*, 394.
(147) Zhang, Y.; Wang, T. H. *Theranostics* **2012**, *2*, 631.
(148) Medintz, I. L.; Clapp, A. R.; Brunel, F. M.; Tiefenbrunn, T.; Uyeda, H. T.; Chang, E. L.; Deschamps, J. R.; Dawson, P. E.; Mattoussi, H. *Nat. Mater.* **2006**, *5*, 581.
(149) Freeman, R.; Finder, T.; Gill, R.; Willner, I. *Nano Lett.* **2010**, *10*, 2192.
(150) Prasuhn, D. E.; Feltz, A.; Blanco-Canosa, J. B.; Susumu, K.; Stewart, M. H.; Mei, B. C.; Yakovlev, A. V.; Loukov, C.; Mallet, J.-M.; Oheim, M.; Dawson, P. E.; Medintz, I. L. *ACS Nano* **2010**, *4*, 5487.
(151) Algar, W. R.; Malanoski, A. P.; Susumu, K.; Stewart, M. H.; Hildebrandt, N.; Medintz, I. L. *Anal. Chem.* **2012**, *84*, 10136.
(152) Lowe, S. B.; Dick, J. A. G.; Cohen, B. E.; Stevens, M. M. *ACS Nano* **2012**, *6*, 851.
(153) Willard, D. M.; Carillo, L. L.; Jung, J.; Van Orden, A. *Nano Lett.* **2001**, *1*, 469.
(154) Clapp, A. R.; Medintz, I. L.; Mauro, J. M.; Fisher, B. R.; Bawendi, M. G.; Mattoussi, H. *J. Am. Chem. Soc.* **2004**, *126*, 301.
(155) Goldman, E. R.; Medintz, I. L.; Mattoussi, H. *Anal. Bioanal. Chem.* **2006**, *384*, 560.
(156) Kattke, M. D.; Gao, E. J.; Sapsford, K. E.; Stephenson, L. D.; Kumar, A. *Sensors* **2011**, *11*, 6396.
(157) Qian, J.; Wang, C. Q.; Pan, X. H.; Liu, S. Q. *Anal. Chim. Acta* **2013**, *763*, 43.
(158) Zhou, D.; Piper, J. D.; Abell, C.; Klenerman, D.; Kang, D.-J.; Ying, L. *Chem. Commun.* **2005**, *38*, 4807.
(159) Cheng, A. K. H.; Su, H.; Wang, A.; Yu, H.-Z. *Anal. Chem.* **2009**, *81*, 6130.
(160) Freeman, R.; Li, Y.; Tel-Vered, R.; Sharon, E.; Elbaz, J.; Willner, I. *Analyst* **2009**, *134*, 653.
(161) Wu, C.-S.; Cupps, J. M.; Fan, X. *Nanotechnology* **2009**, *20*, 305502.
(162) Tavares, A. J.; Noor, M. O.; Vannoy, C. H.; Algar, W. R.; Krull, U. J. *Anal. Chem.* **2012**, *84*, 312.
(163) Zhou, D. J. *Biochem. Soc. Trans.* **2012**, *40*, 635.
(164) Snee, P. T.; Somers, R. C.; Nair, G.; Zimmer, J. P.; Bawendi, M. G.; Nocera, D. G. *J. Am. Chem. Soc.* **2006**, *128*, 13320.
(165) Zhang, F.; Ali, Z.; Amin, F.; Feltz, A.; Oheim, M.; Parak, W. J. *ChemPhysChem* **2010**, *11*, 730.

(166) Dennis, A. M.; Rhee, W. J.; Sotto, D.; Dublin, S. N.; Bao, G. *ACS Nano* **2012**, *6*, 2917.
(167) Goldman, E. R.; Clapp, A. R.; Anderson, G. P.; Uyeda, H. T.; Mauro, J. M.; Medintz, I. L.; Mattoussi, H. *Anal. Chem.* **2004**, *76*, 684.
(168) Freeman, R.; Girsh, J.; Jou, A. F. J.; Ho, J. A. A.; Hug, T.; Dernedde, J.; Willner, I. *Anal. Chem.* **2012**, *84*, 6192.
(169) Jaiswal, J. K.; Goldman, E. R.; Mattoussi, H.; Simon, S. M. *Nat. Methods* **2004**, *1*, 73.
(170) Arya, H.; Kaul, Z.; Wadhwa, R.; Taira, K.; Hirano, T.; Kaul, S. C. *Biochem. Biophys. Res. Commun.* **2005**, *329*, 1173.
(171) Michalet, X.; Pinaud, F. F.; Bentolila, L. A.; Tsay, J. M.; Doose, S.; Li, J. J.; Sundaresan, G.; Wu, A. M.; Gambhir, S. S.; Weiss, S. *Science* **2005**, *307*, 538.
(172) Liu, W.; Howarth, M.; Greytak, A. B.; Zheng, Y.; Nocera, D. G.; Ting, A. Y.; Bawendi, M. G. *J. Am. Chem. Soc.* **2008**, *130*, 1274.
(173) Kikkeri, R.; Lepenies, B.; Adibekian, A.; Laurino, P.; Seeberger, P. H. *J. Am. Chem. Soc.* **2009**, *131*, 2110.
(174) Walling, M.; Novak, J.; Shepard, J. R. E. *Int. J. Mol. Sci.* **2009**, *10*, 441.
(175) Coto-Garcia, A. M.; Sotelo-Gonzalez, E.; Fernandez-Argueelles, M. T.; Pereiro, R.; Costa-Fernandez, J. M.; Sanz-Medel, A. *Anal. Bioanal. Chem.* **2011**, *399*, 29.
(176) Delehanty, J. B.; Bradburne, C. E.; Susumu, K.; Boeneman, K.; Mei, B. C.; Farrell, D.; Blanco-Canosa, J. B.; Dawson, P. E.; Mattoussi, H.; Medintz, I. L. *J. Am. Chem. Soc.* **2011**, *133*, 10482.
(177) Boeneman, K.; Delehanty, J. B.; Blanco-Canosa, J. B.; Susumu, K.; Stewart, M. H.; Oh, E.; Huston, A. L.; Dawson, G.; Ingale, S.; Walters, R.; Domowicz, M.; Deschamps, J. R.; Algar, W. R.; DiMaggio, S.; Manono, J.; Spillmann, C. M.; Thompson, D.; Jennings, T.; Dawson, P. E.; Medintz, I. L. *ACS Nano* **2013**, *7*, 3778.
(178) Clapp, A. R.; Medintz, I. L.; Fisher, B. R.; Anderson, G. P.; Mattoussi, H. *J. Am. Chem. Soc.* **2005**, *127*, 1242.
(179) Morgner, F.; Geißler, D.; Stufler, S.; Butlin, N. G.; Löhmannsröben, H.-G.; Hildebrandt, N. *Angew. Chem., Int. Ed.* **2010**, *49*, 7570.
(180) Wegner, K. D.; Lanh, P. T.; Jennings, T.; Oh, E.; Jain, V.; Fairclough, S. M.; Smith, J. M.; Giovanelli, E.; Lequeux, N.; Pons, T.; Hildebrandt, N. *Appl. Mater. Interfaces* **2013**, *5*, 2881.
(181) Wegner, K. D.; Jin, Z.; Lindén, S.; Jennings, T.; Hildebrandt, N. *ACS Nano* **2013**, *7*, 7411.
(182) Wegner, K. D.; Lindén, S.; Jin, Z.; Jennings, T.; El Khoulati, R.; Van Bergen en Henegouwen, P. M. P.; Hildebrandt, N. *Small* **2013**, DOI: 10.1002/smll.201302383.
(183) Morgner, F.; Stufler, S.; Geißler, D.; Medintz, I. L.; Algar, W. R.; Susumu, K.; Stewart, M. H.; Blanco-Canosa, J. B.; Dawson, P. E.; Hildebrandt, N. *Sensors* **2011**, *11*, 9667.
(184) Algar, W. R.; Wegner, D.; Huston, A. L.; Blanco-Canosa, J. B.; Stewart, M. H.; Armstrong, A.; Dawson, P. E.; Hildebrandt, N.; Medintz, I. L. *J. Am. Chem. Soc.* **2012**, *134*, 1876.